Materials Today Chemistry 53 (2026) 103587

Contents lists available at ScienceDirect

Materials Today Chemistry

journal homepage: www.journals.elsevier.com/materials-today-chemistry/

On the comparison between organic batch and aqueous microfluidic PEG-Jeffamine nanogels synthesis for sustained drug release

Giuseppe Nunziata [a], Fabio Pizzetti [a], Valeria Veneruso [b], Arianna Rossetti [a], Emilia Petillo [a,b], Enrico Frigerio [b], Chiara Marabelli [c,d], Mattia Tiboni [e], Luca Casettari [e], Pietro Veglianese [b], Alessandro Sacchetti [a], Filippo Rossi [a,*]

[a] Department of Chemistry, Materials and Chemical Engineering "Giulio Natta", Politecnico di Milano, piazza Leonardo da Vinci 32, 20133, Milan, Italy
[b] Department of Acute Brain and Cardiovascular Injury, Istituto di Ricerche Farmacologiche Mario Negri IRCCS, via Mario Negri 2, 20156, Milano, Italy
[c] Laboratory of Molecular Cardiology, IRCCS Maugeri, 27100, Pavia, Italy
[d] Molecular Medicine Dept, University of Pavia, 27100, Pavia, Italy
[e] Department of Biomolecular Sciences, University of Urbino Carlo Bo, Via Ca le Suore 2, 61029, Urbino, Italy

ARTICLE INFO

Keywords:
Microfluidics
Nanogel
Drug delivery
poly(ethylene glycol)
Jeffamine

ABSTRACT

Nanogels represent an emerging class of soft nanomaterials capable of combining high water content, structural versatility, and tunable responsiveness, making them increasingly attractive for advanced drug delivery applications. Here, we present a modular and fully aqueous strategy to generate fluorescent PEG-Jeffamine nanogels through the integration of orthogonal click chemistry with a continuous-flow microfluidic platform. Unlike conventional emulsification-sonication-evaporation methods, which rely on poorly controlled mixing and often yield modest encapsulation efficiencies, the microfluidic approach provides a scalable and reproducible hydrodynamic environment that enables precise control over network formation, particle morphology, and in-line drug loading. Using FITC (hydrophobic) and RhB (hydrophilic) as model compounds, we demonstrate that the simultaneous synthesis-and-loading configuration (flow/flow) markedly enhances encapsulation efficiency and reduces early burst release compared with all batch-derived formulations. Specifically, the encapsulation efficiency increased from 54.2% to 84.9% for FITC and from 92.1% to 95.9% for RhB when moving from batch/batch to flow/flow processing. Structural and morphological analyses (DLS, Cryo-TEM) confirm the formation of monodisperse nanogels with controlled nanoscale dimensions (90-110 nm), while quantitative image analysis reveals a significantly higher particle circularity for flow-synthesized nanogels, indicating improved shape regularity. In addition, EDS analysis verifies the retention of reactive moieties that enable further post-synthetic functionalization. Overall, this work introduces a scalable and water-based microfluidic workflow for producing multifunctional PEG-Jeffamine nanogels with enhanced drug loading, sustained release, improved morphological uniformity, and reduced cytotoxicity, offering a promising platform for high-dose and long-term therapeutic applications.

1. Introduction

In recent years, advancements in nanobiotechnology have enabled the development of innovative materials capable of transforming drug administration and biodistribution [1,2]. Among these, nanogels have emerged as one of the most versatile and promising platforms for drug delivery, owing to their unique ability to amalgamate the properties of hydrogels and nanoparticles [3]. Defined as highly cross-linked nanometric hydrogels, nanogels possess a three-dimensional porous network capable of retaining large amounts of water without dissolving [4,5]. This distinctive structure renders nanogels well suited for encapsulating small molecules, proteins, peptides, and nucleic acids [6]. Furthermore, their mechanical and chemical properties can be fine-tuned to optimize drug-loading capabilities and release kinetics, rendering them ideal candidates for applications in oncology [7], gene therapy [8], vaccination [9], neurodegenerative disease therapy [10], and regenerative medicine [11]. Moreover, the possibility to tune their responsiveness to pH, temperature, ionic strength, and light enables controlled drug

* Corresponding author.
E-mail address: filippo.rossi@polimi.it (F. Rossi).

https://doi.org/10.1016/j.mtchem.2026.103587
Received 19 January 2026; Received in revised form 31 March 2026; Accepted 1 April 2026
Available online 3 April 2026

release, and their surface decoration allows targeted cellular uptake [12–14]. Within cationic nanogel platforms, polyethyleneimine (PEI)--based systems have long represented the gold standard due to their positive charge leading to strong nucleic acid complexation [15–17]. However, their non-degradable nature and high density charge cause dose-dependent membranes disrupture, cytotoxicity and inflammatory responses [18,19]. In high concentration regimes, PEI-based systems can induce significant cell death and immunogenic responses, undermining their safety profile [20]. This challenge has prompted the search for alternative cationic polymers that provide the benefits of PEI, effective payload binding and release, with improved safety [21–23]. Jeffamine, a class of polyetheramines, has recently gained attention as a promising alternative. Its polyethylene oxide/polypropylene oxide (PEO/PPO) backbone confers high hydrophilicity, reduced cytotoxicity, and tunable physicochemical properties, while maintaining efficient cellular interaction [24]. Comparative studies have shown that PEG (poly(ethylene glycol))-Jeffamine nanogels exhibit smaller sizes and improved colloidal stability relative to PEG-PEI analogues [25].

However, reported encapsulation efficiencies remain heterogeneous and often modest (40-70%), strongly depending on the synthesis and loading conditions [26,27]. To address these limitations, microfluidics has emerged as a powerful strategy for nanomaterial manufacturing [28,29]. Unlike bulk emulsification or nanoprecipitation, which suffer from uncontrolled mixing and batch-to-batch variability, microfluidic reactors provide continuous and reproducible hydrodynamic environments that improve nucleation, mass transfer and encapsulation efficiency [30,31]. Several microfluidic modalities have been explored, including solvent-antisolvent nanoprecipitation, self-assembly driven by pH or temperature gradients, and droplet-based systems that generate highly uniform reaction microenvironments [32–34]. While these approaches have shown improved control over particle formation, their application to polymeric nanogels remains limited, and most studies still rely on inorganic or hybrid systems [35]. Moreover, ionic-gelation nanogels produced in flow, although achieving excellent encapsulation efficiencies, are constrained by the requirement for charged biopolymers and electrostatic crosslinking, limiting their applicability and long-term stability [36]. For example, lipid nanoparticles produced via hydrodynamic flow-focusing exhibited more than 20 % higher encapsulation efficiency relative to vortex-mixed systems [37]. Similarly, Shepherd and coworkers developed a coaxial flow reactor to continuously produce lysozyme-loaded chitosan nanogels, achieving excellent size control and encapsulation efficiencies up to 94.6 ± 2.9 % substantially higher and more reproducible than those typically obtained via batch ionic gelation [38]. However, ionic-gelation remains constrained by the need for charged biopolymers and electrostatic interactions, limiting drug compatibility and long-term stability [39]. Herein, we introduce a distinct microfluidic strategy that integrates a covalent crosslinking reaction into a fully aqueous, continuous-flow environment, enabling simultaneous nanogel formation and drug encapsulation without organic solvents. This approach bridges the gap between Jeffamine-based biocompatibility and the manufacturing precision of flow chemistry, offering a scalable and reproducible platform for PEG-Jeffamine nanogels.

In order to compare the output of the two different approaches in

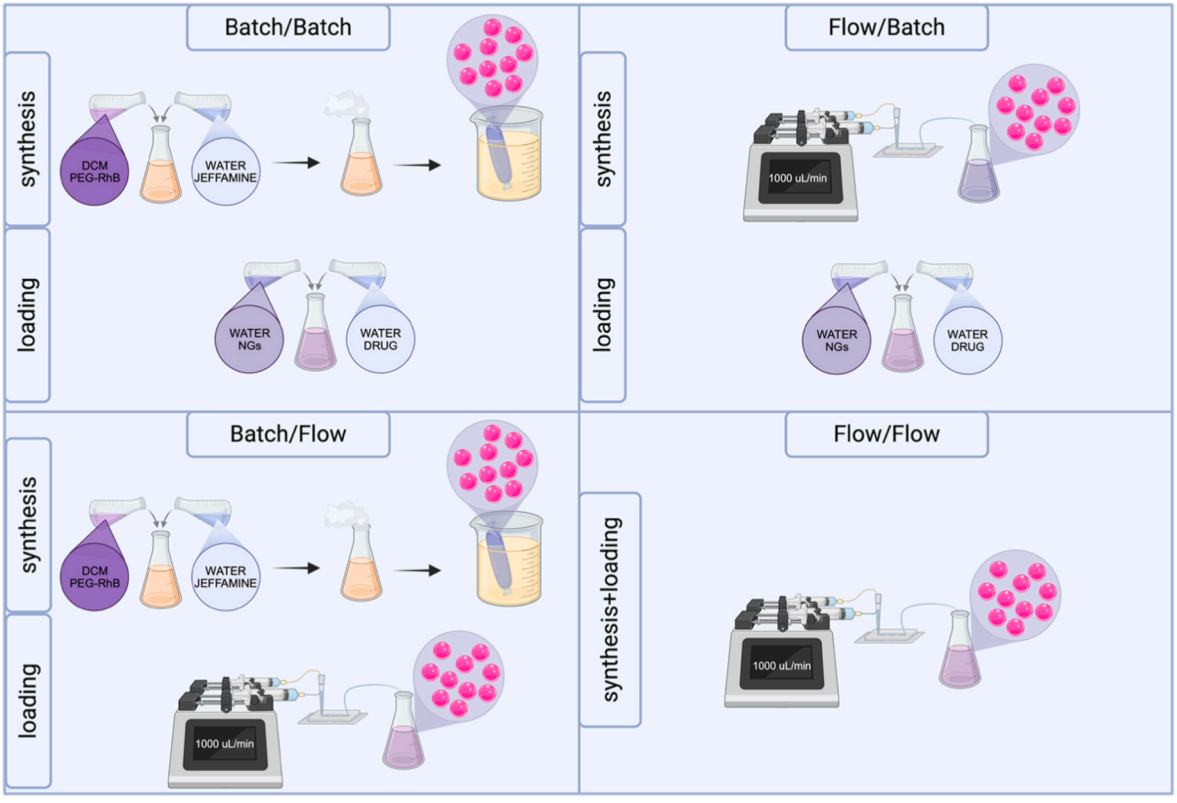

Fig. 1. Each panel represents a distinct combination of synthetic environment (batch or microfluidic flow) and loading modality (batch diffusion or in-flow encapsulation): (a) *Batch/Batch:* Nanogels are synthesized via conventional emulsification-sonication-evaporation in a biphasic dichloromethane (DCM)/water system, followed by solvent evaporation. Drug loading is subsequently performed in batch by mixing aqueous nanogels with an aqueous dye solution under stirring; (b) *Flow/Batch:* Nanogels are synthesized entirely in microfluidics using two aqueous inlet streams (modify-PEG and Jeffamine) injected into a split-and-recombine polypropylene chip. The resulting aqueous nanogels are then subjected to batch loading by mixing with dye solution under static conditions; (c) *Batch/Flow:* Nanogels are first synthesized in batch, and the purified aqueous dispersion is then loaded using the microfluidic chip, where nanogels and dye solution are co-injected to achieve rapid mixing and improved encapsulation efficiency; (d) *Flow/Flow:* Both synthesis and drug loading occur directly within the microfluidic platform. Modify-PEG and Jeffamine streams are co-injected at 1000 μL/min, enabling simultaneous nanogel formation and real-time encapsulation in a fully aqueous, continuous-flow environment.

each step (*i.e.* synthesis and drug loading), four cases were investigated (Fig. 1), combining either *in batch* or *in flow* procedures.

Finally, we demonstrated that continuous-flow synthesis coupled with in-line drug loading (flow/flow) provides precise control over nanogel size, dispersity, and internal architecture, resulting in markedly enhanced encapsulation efficiency for both hydrophilic and hydrophobic compounds. The resulting nanogels show minimal burst release and a more homogeneous distribution of payload within the polymeric network, features essential for high-dose therapeutic applications.

2. Materials and methods

2.1. Materials and machines

Polyethylene glycol 8000 (PEG 8000, $[C_2H_4O]_n$, MW: 8000 g/mol, Sigma-Aldrich), Epichlorohydrin (C_3H_5ClO, MW: 92.52 g/mol, ≥99%, Sigma-Aldrich), Sodium hydroxide (NaOH, MW: 40.00 g/mol, ≥98%, Sigma-Aldrich), Toluene ($C_6H_5CH_3$, MW: 92.14 g/mol, ≥99.5%, Carlo Erba), Dichloromethane (DCM, CH_2Cl_2, MW: 84.93 g/mol, ≥99.8%, Carlo Erba), Deionized water (H_2O, MW: 18.015 g/mol), Sodium sulfate (Na_2SO_4, anhydrous, MW: 142.04 g/mol, ≥99%, Acros Organics), Diethyl ether ($C_4H_{10}O$, MW: 74.12 g/mol, ≥99.7%, Carlo Erba), Deuterated chloroform ($CDCl_3$, MW: 120.38 g/mol, ≥99.8% D, Sigma-Aldrich), Deuterium oxyde (D_2O, 99%, CIL), Sodium azide (NaN_3, MW: 65.01 g/mol, ≥99.5%, Sigma-Aldrich), Ammonium chloride (NH_4Cl, MW: 53.49 g/mol, ≥99.5%, Sigma-Aldrich), N,N-Dimethylformamide (DMF, C_3H_7NO, MW: 73.09 g/mol, ≥99.8%, Sigma-Aldrich), Acetone (C_3H_6O, MW: 58.08 g/mol, ≥99.5%, Carlo Erba), rhodamine B (RhB, $C_{28}H_{31}ClN_2O_3$, MW: 479.96 g/mol, Sigma-Aldrich), Ethylenediamine ($C_2H_4(NH_2)_2$, MW: 60.10 g/mol, ≥99%, Sigma-Aldrich), Ethanol (C_2H_5OH, 99,8%, MW = 46.07 g/mol, Carlo Erba), Hydrochloric acid (HCl, MW: 36.46 g/mol, 37%, Sigma-Aldrich), Propargyl bromide (C_3H_3Br, MW: 121.94 g/mol, 80% in toluene, Sigma-Aldrich), Triethylamine (TEA, $N(C_2H_5)_3$, MW: 101.19 g/mol, ≥99%, Sigma-Aldrich), Acetonitrile (ACN, C_2H_3N, MW: 41.05 g/mol, ≥99.9%, Carlo Erba), Propargylamine ($C_3H_5NH_2$, MW: 57.09 g/mol, ≥98%, Sigma-Aldrich), Potassium carbonate (K_2CO_3, MW: 138.21 g/mol, ≥99%, Sigma-Aldrich), Methanol (MeOH, CH_4O, MW: 32.04 g/mol, ≥99.9%, Carlo Erba), Copper(I) iodide (CuI, MW: 190.45 g/mol, ≥99.5%, Alfa Aesar), L-Ascorbic acid sodium salt ($C_6H_7NaO_6$, MW: 198.11 g/mol, ≥99%, Acros Organics), Carbonyldiimidazole (CDI, $C_7H_6N_4O$, MW: 130.10 g/mol, ≥97%, Sigma-Aldrich), Jeffamine 2000 (Polyetheramine, MW: 2000 g/mol, Huntsman), Fluorescein Isothiocyanate, isomer I (FITC, $C_{21}H_{11}NO_5S$, MW: 389.38 g/mol, ≥99%, Sigma-Aldrich), Dimethyl sulfoxide (DMSO, $(CH_3)_2SO$, MW: 78.13 g/mol, ≥99.9%, Sigma-Aldrich), 2-Aminoethanethiol (C_2H_7NS, MW: 77.16 g/mol, ≥98%, Sigma-Aldrich), Methyl iodide (CH_3I, MW: 141.94 g/mol, ≥99%, Sigma-Aldrich), Benzyl chloride ($C_6H_5CH_2Cl$, MW: 127.58 g/mol, ≥99%, Sigma-Aldrich), 1,4-Dioxane ($C_4H_8O_2$, MW: 88.11 g/mol, ≥99.8%, Sigma-Aldrich), 4-Toluenesulfonyl chloride ($CH_3C_6H_4SO_2Cl$, MW: 190.65 g/mol, ≥99%, Sigma-Aldrich). All solvents were of analytical grade purity and used without further treatment.

2.1.1. Nuclear Magnetic Resonance (NMR) analysis

Reaction intermediates and final products were characterized by Nuclear Magnetic Resonance spectroscopy (^1H and ^{13}C NMR) using a Bruker AC spectrometer (500 MHz, Bruker Corp., Billerica, MA, USA). Deuterated chloroform ($CDCl_3$) was used as solvent, and chemical shifts were reported in ppm relative to the residual solvent signal.

2.1.2. Attenuated Total Reflectance Fourier Transform Infrared (FTIR) analysis

Attenuated Total Reflectance Fourier Transform Infrared spectroscopy (FTIR) was performed using a Thermo Nexus 6700 spectrometer coupled to a Thermo Nicolet Continuum infrared microscope equipped with a 15 × Reflachromat Cassegrain objective (Thermo Fisher Scientific, Waltham, MA, USA). Spectra were acquired at room temperature in air with 32 accumulated scans in the wavenumber range of 4000–800 cm^{-1} at a resolution of 4 cm^{-1}.

2.1.3. Dynamic Light Scattering (DLS) analysis

The hydrodynamic diameter, polydispersity index (PDI), and ζ-potential of the nanogels were measured by Dynamic Light Scattering (DLS) using a Zetasizer Nano ZS instrument (Malvern Panalytical, Malvern, UK). Samples were dispersed in PBS solution at a concentration of 1 mg mL^{-1}. All measurements were performed in triplicate.

2.1.4. Gel Permeation Chromatography (GPC)

Molecular weight distribution of the PEG-based and Jeffamine-based polymers was determined by Gel Permeation Chromatography (GPC), also known as Size Exclusion Chromatography (SEC). Analyses were performed using tetrahydrofuran (THF) as the eluent at a flow rate of 1 mL min^{-1} and a column temperature of 35 °C. Polymer samples were dried under vacuum and subsequently dissolved in a mixture of 10% DMF+ 90% THF to obtain a final concentration of 4 mg mL^{-1}. The solutions were filtered through a 0.45 μm PTFE membrane filter prior to injection. The chromatographic system (Jasco 2000 series) was equipped with a differential refractive index (RI) detector and three PLgel columns (Polymer Laboratories Ltd., UK), including two mixed-bed MXC columns and one Oligopore column (300 mm length × 7.5 mm internal diameter), together with a precolumn. Calibration was carried out using polystyrene (PS) standards with molecular weights ranging from 580 Da to 3,250,000 Da (Polymer Laboratories).

2.1.5. Cryogenic Transmission Electron Microscopy (Cryo-TEM)

Morphological and topographical analyses of the nanogels were carried out using Cryogenic Transmission Electron Microscopy (Cryo-TEM). Samples were vitrified using a Mark IV Vitrobot operated at 4 °C and 100% relative humidity. For each sample, 3.5 μL of suspension were deposited onto Quantifoil R2/1 Cu 300-mesh grids previously glow-discharged at 30 mA for 30 s using a GloQube system. The grids were blotted and plunge-frozen in liquid ethane. Cryo-TEM images were acquired using a Talos Arctica microscope operating at 200 kV and equipped with a Falcon 3 direct electron detector, with a defocus range of −3.0 to −4.0 μm and a total electron dose of 40 $e^- Å^{-2}$. Particle size distributions were determined by processing the micrographs using ImageJ software.

2.2. Synthesis of diepoxy-PEG **(1)**

Polyethylene glycol 8000 (PEG) (2.0 g, 0.25 mmol, 1eq.) was dissolved in 12 mL of toluene and stirred at room temperature until complete dissolution. Epichlorohydrin (0.694 g, 7.5 mmol, 30 eq.) was added dropwise, followed by powder of sodium hydroxide (0.300 g, 7.5 mmol, 30 eq.). The mixture was heated at 50 °C for 7 h under constant stirring. After cooling to room temperature, toluene was removed under reduced pressure. The crude product was purified by liquid-liquid extraction using a brine/deionized water mixture (3:1 v/v) and Dichloromethane (DCM) (40 mL, three times). The organic phase was dried over anhydrous sodium sulfate (Na_2SO_4), filtered, and concentrated. The final polymer, named diepoxy-PEG, was precipitated in diethyl ether, collected by vacuum filtration, and dried. ^1H NMR spectra were recorded on a Bruker 400 MHz spectrometer using deuterated chloroform ($CDCl_3$) (Fig. S1).

2.3. Synthesis of PEG-N_3 **(2)**

Diepoxy-PEG **(1)** (800 mg, 0.1 mmol, 1 eq.) was dissolved in 15 mL of N,N-Dimethylformamide (DMF) under stirring. Sodium azide (130 mg, 1.8 mmol, 18 eq.) and ammonium chloride (216 mg, 3.6 mmol, 36 eq.) were added, and the mixture was stirred at 60 °C for 48 h. After cooling, inorganic salts were removed by vacuum filtration, and the

filter cake was washed with DCM (10 mL). The combined organic phases were concentrated under reduced pressure, and the crude product was purified by liquid-liquid extraction (H_2O/brine and DCM, 3 × 20 mL). The DCM phase was dried and concentrated, and the product was further purified by selective precipitation in diethyl ether. The resulting solid was collected by vacuum filtration and dried. ^{1}H NMR in $CDCl_3$ confirmed PEG-azide (PEG-N_3) **(2)** synthesis (Fig. S2).

2.4. Synthesis of RhB-EDA **(3)**

Rhodamine (RhB) functionalization with ethylenediamine was performed following the procedures discussed in previous works [40,41].

Rhodamine B (600 mg, 1.25 mmol, 1 eq.) was dissolved in 15 mL of absolute ethanol under stirring. Ethylenediamine (2.46 g, 41 mmol, 33 eq.) was added dropwise at RT, and the reaction was then stirred at 110 °C for 24 h in the dark. After completion, ethanol was removed under reduced pressure, and the residue was redissolved in 15 mL of 1 M HCl to remove any unreacted ethylenediamine molecules. Successively, 1 M NaOH (23 mL) was slowly added and the resulting precipitate was recovered by filtration, washed with water (3 × 10 mL) and dried to get the final product Rhodamine B-ethylenediamine (RhB-EDA) **(3)**. ^{1}H NMR in $CDCl_3$ confirmed the formation of RhB-EDA (Fig. S3).

2.5. Synthesis of propargyl RhB-EDA **(4)**

RhB-EDA **(3)** (450 mg, 0.94 mmol, 1 eq.) was dissolved in 15 mL of acetonitrile (ACN) and stirred at 0 °C. Triethylamine (18 mg, 0.18 mmol, 1.25 eq.) was added, followed by dropwise addition of propargyl bromide (21 mg, 0.18 mmol, 1.25 eq.). The mixture was stirred at room temperature for 16 h. After completion, the solvent was removed under reduced pressure, and the crude residue was dissolved in diluted HCl (20 mL, pH ~3). The aqueous phase was extracted with DCM (3 × 40 mL), and the combined organic layers were dried over Na_2SO_4, filtered, and concentrated under vacuum to afford the N-propargylated product. ^{1}H NMR analysis confirmed in $CDCl_3$ successful alkylation (Fig. S4).

2.6. Synthesis of PEG-RhB **(5)**

PEG-azide **(2)** (480 mg, 0.096 mmol, 1 eq.) was dissolved in deionized water (10 mL) and stirred until fully solubilized. Propargyl RhB-EDA **(4)** (46 mg, 0.096 mmol, 1 eq.) was added, followed by catalytic CuI (1 mg) and excess sodium ascorbate (2 mg). The Cu(I)-catalyzed azide-alkyne cycloaddition (CuAAC) was carried out at 50 °C for 24 h under light-protected conditions. Unreacted dye and impurities were removed by dialysis (MWCO 3.5 kDa) against 2 L of acidic saline water at pH 4.1 (5.6 g NaCl + 2 drops 1 M HCl in 1 L H_2O) for 24 h, with periodic medium replacement.

The dialyzed product was frozen (−20 °C) and lyophilized to obtain PEG-RhB as a dry powder. ^{1}H NMR ($CDCl_3$) confirmed successful triazole formation (Fig. S5).

2.7. Synthesis of PEG-CDI-RhB **(6)**

PEG-RhB **(5)** (454 mg, 0.045 mmol, 1 eq.) and unmodified PEG (1000 mg, 0.125 mmol, 1 eq.) were separately activated with 1,1′-carbonyldiimidazole (CDI) in acetonitrile (ACN). For PEG-RhB **(5)**, CDI (90 mg, 0.56 mmol, 12.5 eq.) was added to a 10 mL ACN solution and stirred at 40 °C for 24 h. For unmodified PEG, CDI (203.74 mg, 0.45 mmol, 10 eq.) was added to 40 mL of ACN and stirred under identical conditions. After reaction completion, ACN was removed under reduced pressure. The residue was cooled in an ice bath and precipitated with diethyl ether. The solid was collected by vacuum filtration and dried. ^{1}H NMR ($CDCl_3$) confirmed successful CDI bonding (Fig. S6).

2.8. Synthesis of PEG-based nanogels via crosslinking with Jeffamine **(7)**

2.8.1. Batch synthesis via emulsification-sonication-evaporation

PEG-Jeffamine nanogels were prepared through a conventional emulsification-sonication-evaporation process. PEG-CDI (1.0 g, 0.125 mmol, 1 eq.) was dissolved in 1.5 mL dichloromethane (DCM) and added dropwise to 3 mL of an aqueous Jeffamine solution (2.5 g, 1.25 mmol, 10 eq.) under vigorous stirring (600 rpm). Fluorescent nanogels were prepared analogously using PEG-CDI-RhB **(6)** (40 mg, 0.0045 mmol) and Jeffamine (94 mg, 0.047 mmol) under identical conditions. The biphasic mixture was sonicated for 30 min to promote emulsification, followed by overnight stirring to allow solvent evaporation and network formation. Hydrodynamic diameter, polydispersity index, and zeta potential were measured by DLS. Morphology was assessed by Cryo-TEM.

2.8.2. Microfluidic synthesis in a fully aqueous split-and-recombine micromixer

For the continuous-flow approach, a previously developed 3D-printed split-and-recombine (SAR) microfluidic chip was employed to enable in-flow nanogel formation under fully aqueous conditions. The chip was fabricated by fused deposition modeling using an Ultimaker 3 3D printer (Ultimaker, The Netherlands) loaded with a polypropylene filament (BASF, Germany). Its structure was optimized to achieve effective passive micromixing through “split-and-recombine” circular asymmetric channels, designed with alternating widths of 0.4 mm and 0.6 mm and a channel height of 1 mm [42]. Two aqueous streams were infused into the microfluidic chip using syringe pumps. Preliminary optimization experiments were performed by varying the equal inlet flow rates over a range of 100-4000 μL min^{-1} (100/100, 500/500, 1000/1000, 1500/1500, 2000/2000, 3000/3000, and 4000/4000 μL min^{-1}), while maintaining a constant flow rate ratio of 1:1. Among these conditions, a flow rate of 1000/1000 μL min^{-1} produced nanogels with the lowest polydispersity index and was therefore selected for all subsequent experiments. Under the optimized conditions, two aqueous streams were infused into the chip at equal flow rates of 1000 μL min^{-1} each (total flow rate 2000 μL min^{-1}, flow rate ratio 1:1). The first stream contained PEG-CDI-RhB **(6)** at a concentration of 0.67 mg mL^{-1}, while the second stream contained Jeffamine at 1.57 mg mL^{-1}. The outlet suspension was collected and lyophilized.

2.9. Synthesis of the sulfur-containing probe **(9)** (p-toluenesulfonyl-propargylamine derivative) and PEG azide groups quantification

To introduce a quantifiable sulfur marker, *p*-toluenesulfonyl-propargylamine was synthesized by sulfonylation of propargylamine. Propargylamine (1.3 mL, 18.1 mmol, 1 eq.) was dissolved in 35 mL of anhydrous dichloromethane (DCM) under magnetic stirring at 0 °C. Triethylamine (7 mL, 50.2 mmol, 2.8 eq.) was added dropwise to maintain basic conditions. In parallel, *p*-toluenesulfonyl chloride (3.8 g, 20.0 mmol, 1.1 eq.) was dissolved in 15 mL of DCM and added dropwise to the reaction mixture while maintaining the temperature at 0 °C.

After 1 h of stirring, the solvent was removed under reduced pressure, and the crude residue was dissolved in 200 mL of diethyl ether. The organic phase was washed twice with 50 mL of 1 M HCl and once with 30 mL of saturated NH_4Cl solution. The ether layer was dried over anhydrous Na_2SO_4, filtered, and concentrated under vacuum to yield the purified product, assessed through 1H NMR analysis (Fig. S7). To quantify accessible azide groups, the synthesized *p*-toluenesulfonyl-propargylamine was conjugated via CuAAC to three PEG-azide systems: unmodified PEG-azide (reference), partially functionalized PEG-RhB (50%), and fully functionalized PEG-RhB (100%). The CuAAC reaction with the sulfur-containing probe was performed on PEG-based polymer precursors prior to nanogel formation. To ensure efficient conversion of the accessible azide groups, the CuAAC reaction was performed using the PEG-based substrate (480 mg, 0.096 mmol, 1 eq.) and *p*-toluenesulfonyl-propargylamine (201 mg, 0.96 mmol, 10 eq.) as the alkyne

partner in excess. The excess of the alkyne probe ensured efficient reaction with the remaining accessible azide groups and minimized incomplete conversion during the click reaction. Reactions were performed under standard CuAAC conditions using copper(I) iodide (1 mg) and sodium ascorbate (2 mg) in aqueous medium. After purification via dialysis, sulfur content was quantified by energy-dispersive X-ray spectroscopy (EDS). The sulfur signal was correlated to the amount of residual azide groups, providing insight into the efficiency of rhodamine B conjugation and the extent of free site availability across different PEG architectures.

2.10. Post-functionalization PEG-RhB-Jeffamine NGs with propargylamine

PEG-RhB-Jeffamine NGs were further post-functionalized to introduce primary amine functionalities. This was achieved through a Cu(I)-catalyzed azide-alkyne cycloaddition (CuAAC) reaction using propargylamine as the alkyne partner. Briefly, PEG-RhB-Jeffamine NGs (480 mg, 0.067 mmol, 1 eq.) was dissolved in 15 mL of deionized water under inert atmosphere, and propargylamine (7.37 mg, 0.134 mmol, 2 eq.) was added in excess with respect to the residual azide groups.

Reactions were performed under standard CuAAC conditions using copper(I) iodide (1 mg) and sodium ascorbate (2 mg) in aqueous medium. The reaction mixture was stirred at 50 °C for 36 h, allowing efficient conversion of azide groups into stable 1,4-disubstituted 1,2,3-triazole linkages bearing terminal primary amines. Upon completion, the reaction mixture was purified by extensive dialysis against deionized water to remove copper salts, unreacted small molecules, and by-products, followed by lyophilization to obtain the amine-functionalized NGs.

2.11. Drug release studies

To investigate the release behaviour of the synthesized PEG-Jeffamine nanogels using a membrane diffusion method [43], two model compounds with different physicochemical properties were selected: rhodamine B as a hydrophilic probe, and fluorescein isothiocyanate (FITC, isomer I) as a moderately hydrophobic one [44–46]. Drug loading was carried out using PEG-Jeffamine nanogels prepared through four distinct fabrication modes: batch/batch, flow/batch, batch/flow, and flow/flow. For all loading experiments, nanogels were suspended in phosphate-buffered saline (PBS, pH 7.4) at a final concentration of 20 mg mL^{-1}, while both rhodamine B (RhB) and fluorescein isothiocyanate (FITC) were dissolved at 1 mg mL^{-1} in the same medium. In the batch/batch and flow/batch systems, drug loading was performed after nanogel synthesis through a passive diffusion approach [25]. Specifically, 1 mL of the drug solution was added dropwise to 1 mL of the nanogel suspension under gentle stirring and the mixture was incubated at room temperature for 17 h to allow diffusion-driven encapsulation and equilibrium partitioning of the dye within the nanogel network. For batch/flow formulations, pre-synthesized nanogels were injected into one inlet of the microfluidic chip, while the drug solution was introduced through the second inlet at equal flow rates (1000 μL min^{-1} each). This configuration enabled rapid micromixing within the split-and-recombine channels and promoted on-chip diffusion-assisted loading of the dye into already formed nanogels. In contrast, the flow/flow configuration was designed to enable simultaneous nanogel formation and drug encapsulation.

In this case, the drug was dissolved directly within the two aqueous inlet streams together with the polymer precursors (each containing 1 mg mL^{-1} of dye and the corresponding PEG-CDI-RhB or Jeffamine solution at 1–3 mg mL^{-1}). Under these conditions, the mixing and cross-linking reactions occurring inside the microfluidic channels allowed the dye molecules to become entrapped in situ during network formation, rather than diffusing into pre-formed nanogels. This one-step strategy represents a key feature of the flow/flow approach, enabling faster processing and improved encapsulation efficiency. After loading, all samples were transferred into dialysis membranes (MWCO 3.5 kDa) and subjected to a pre-washing step by dialyzing against 40 mL of PBS (pH 7.4) for 30 min at room temperature to remove non-encapsulated dye molecules. The washing medium was collected and analyzed by UV-Vis spectrophotometry to quantify any free dye and calculate the encapsulation efficiency (EE %) and drug loading (DL %). The encapsulation efficiency and drug loading were calculated according to the following equations:

$$EE\% = \left(1 - \frac{C_V}{C_0}\right) \cdot 100 \quad (1)$$

$$DL\% = \left(\frac{m_{ed}}{m_{ed} + m_p}\right) \cdot 100 \quad (2)$$

where EE% represents the encapsulation efficiency, C_0 is the initial drug concentration, and C_v is the drug concentration measured in the external medium after the washing step. DL% represents the drug loading, m_{ed} is the mass of encapsulated drug, and m_p is the mass of polymer used for nanogel preparation. Absorbance measurements were recorded at λ = 555 nm for rhodamine B and λ = 494 nm for FITC, using calibration curves prepared in PBS under identical conditions (Fig. S8). Following the washing step, fresh 40 mL of PBS were added to each sample to initiate the in vitro release study, which was carried out at 37 °C under sink conditions with constant gentle agitation. At predetermined time points (1, 2, 4, 6, 8, 24, 48, 72, 96 h, and daily up to 7 days, followed by weekly sampling for 4 weeks), 2 mL aliquots of the external PBS medium were withdrawn and immediately replaced with an equal volume of fresh buffer to maintain constant volume and sink conditions.

The absorbance of each aliquot was measured at the respective λ_max of the dyes, and the cumulative release profiles were constructed by plotting the percentage of dye released relative to the total encapsulated amount.

2.12. Cytotoxicity assessment of PEG-Jeffamine nanogels on oligodendrocytes using LDH assay

The cytotoxicity of fluorescent PEG-Jeffamine nanogels was assessed using the Lactate Dehydrogenase (LDH) assay, which quantifies membrane damage by measuring extracellular LDH release, on primary mixed cell cultures obtained from mouse spinal cord. Cells were obtained through enzymatic and mechanical dissociation of mouse embryos spinal cords and seeded onto a layer of mature astrocytes. The cultures were maintained at 37 °C in a humidified atmosphere, and after 6 days in vitro, a mixed cell population containing astrocytes, oligodendrocytes, neurons, and microglia was established. To simulate a neuroinflammatory environment, the mixed cultures were stimulated with lipopolysaccharide (LPS, 100 ng/mL) as a generic inflammatory stimulus, and after 18 h of activation the cells were treated with PEG-Jeffamine nanogels at two different concentrations (0.05% and 0.005% w/v) for 24 h. Nanogels labelled with rhodamine B were dispersed in culture medium and incubated with the cells for 24 h. After 24 h of nanogel exposure, the culture medium was collected from each well and transferred to a 96-well plate for LDH quantification. Luminescence was measured using a plate reader, and values were normalized against a positive control (cells treated with a cytotoxic agent) and a negative control (untreated cells). Cytotoxicity was expressed as a percentage relative to the positive control group.

2.13. Statistical analysis

The experimental data were analyzed using Analysis of Variance (ANOVA). Statistical significance was set to $p\ value < 0.05$. Results are presented as mean value ± standard deviation.

3. Results and discussion

3.1. Synthesis and chemical characterization

The chemical modification of PEG and RhB was strategically designed to enable site-specific conjugation and subsequent nanogel formation via a modular and orthogonal synthetic route. The initial functionalization of PEG with an azide group was successfully achieved through a two-step process. First, PEG was treated with epichlorohydrin in the presence of sodium hydroxide, yielding epoxide-terminated PEG via nucleophilic substitution, introducing the reactive epoxide moiety. The successful synthesis of diepoxy-PEG **(1)** was confirmed using ^{1}H NMR spectroscopy (Fig. S1). Subsequent nucleophilic ring-opening of the epoxide by sodium azide in DMF led to the formation of PEG-N_3 **(2)**, which exhibited both azide and hydroxyl functionalities. This PEG-N_3 served as a key building block for click chemistry applications. Conversion of diepoxy-PEG **(1)** to PEG-N_3 **(2)** was assessed through ^{1}H NMR spectroscopy (Fig. S2), confirming effective purification [47]. Parallelly, RhB was selectively functionalized with a propargyl group through an amination-alkylation strategy, as outlined in Scheme 1. The introduction of a linker in RhB using EDA enables the possibility to easily couple it with propargyl bromide, useful for further functionalization via "click chemistry". The formation of RhB-EDA **(3)** was confirmed by ^{1}H NMR spectroscopy (Fig. S3), applying a procedure already developed in previous works [40,41]. The subsequent propargyl RhB-EDA **(4)** was obtained via an SN2 reaction between the primary amine in RhB-EDA **(3)** and the electrophilic carbon of the alkyl halide. The successful formation of propargyl RhB-EDA was confirmed by ^{1}H NMR spectroscopy (Fig. S4).

The reaction between propargyl RhB-EDA **(4)** and PEG-N_3 **(2)** yielded PEG-RhB **(5)** with high efficiency and selectivity, forming stable 1,4-disubstituted 1,2,3-triazole linkages. This product retained both the hydrophilic nature of PEG and the optical properties of RhB, confirming successful bioconjugation and laying the foundation for the development of fluorescent nanogels. The successful CuAAC conjugation was confirmed using ^{1}H NMR spectroscopy (Fig. S5). The PEG-RhB **(5)** was subsequently activated using CDI, which yielded imidazolyl carbamate intermediate **(6)** capable of reacting with nucleophilic moieties. Activation proceeded via the nucleophilic attack of PEG hydroxyl groups on the carbonyl carbon of CDI, releasing imidazole as a by-product. The activation of PEG with CDI was confirmed by ^{1}H NMR spectroscopy (Fig. S6). The functionalization route leading from PEG to PEG-RhB-CDI **(6)** is depicted in Scheme 2. The PEG-CDI-RhB and Jeffamine precursors were characterized by NMR, showing molecular weights of approximately 12 kDa and 3.5 kDa, respectively (Fig. S9). The deviation from the expected values can be attributed to the calibration of the measurements based on polystyrene standards.

3.2. Nanogels synthesis and characterization

PEG-Jeffamine nanogels were synthesized through the crosslinking of CDI-activated PEG with Jeffamine in a biphasic system performing the emulsification-sonication-evaporation method [48]. The synthetic method plays a pivotal role in determining nanogel quality, as parameters such as size distribution, colloidal stability, and encapsulation efficiency are highly sensitive to the kinetics of network formation (Scheme 3) [49]. The successful crosslinking between CDI-activated PEG and Jeffamine was confirmed by FTIR spectroscopy (Fig. S10). In particular, the spectrum of the nanogel shows the appearance of a characteristic carbonyl stretching band at ~1700–1720 cm^{-1}, attributed to the formation of carbamate (urethane) linkages. This band is absent in the Jeffamine precursor and confirms the occurrence of the crosslinking reaction. In addition, the broad N–H stretching band observed in the 3300-3500 cm^{-1} region changes significantly after reaction. Compared to the Jeffamine precursor, where primary amine groups are present, the intensity of this region decreases and its shape becomes broader, consistent with the conversion of NH_2 groups into urethane N–H functionalities. Further evidence is provided by the bands in the 1100 cm^{-1} region, corresponding to C–O–C stretching of the PEG backbone, which remain unchanged, indicating preservation of the polymer structure. Overall, the combination of the emergence of carbamate C═O

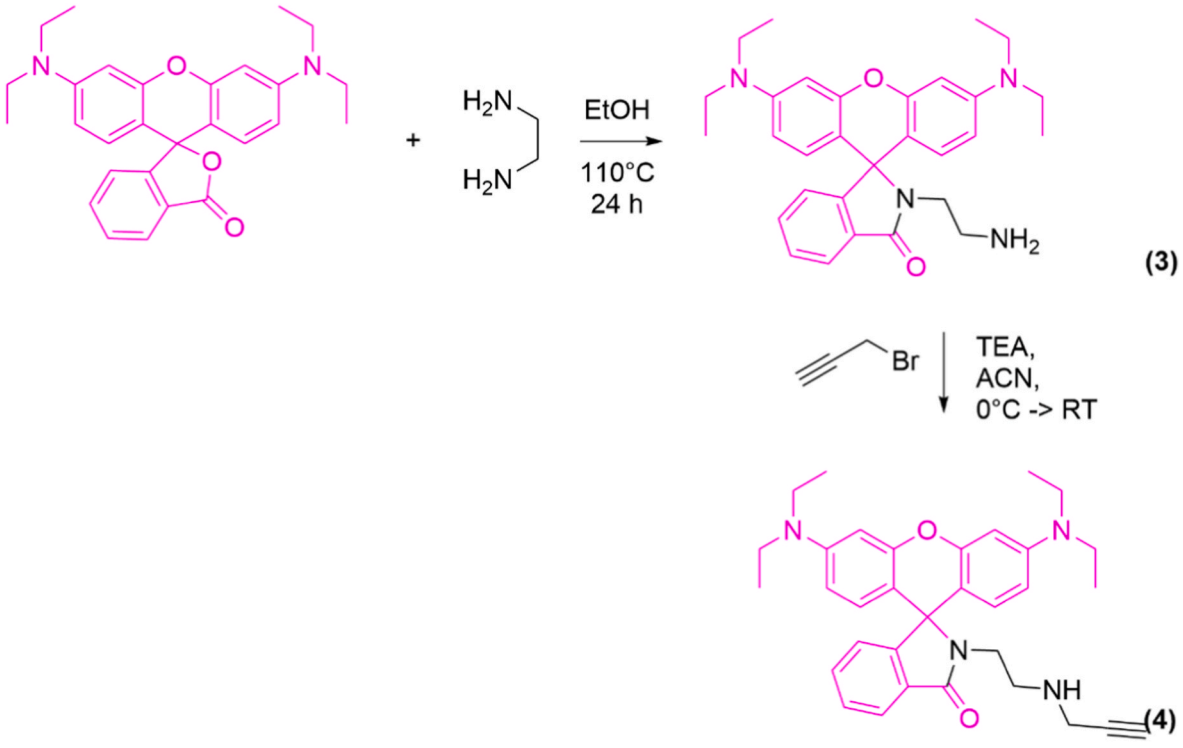

Scheme 1. Two-step functionalization of Rhodamine B. RhB was first converted into RhB-EDA **(3)** via ethylenediamine derivatization, followed by N-propargylation to yield propargyl RhB-EDA **(4)**, introducing a terminal alkyne group suitable for CuAAC click chemistry.

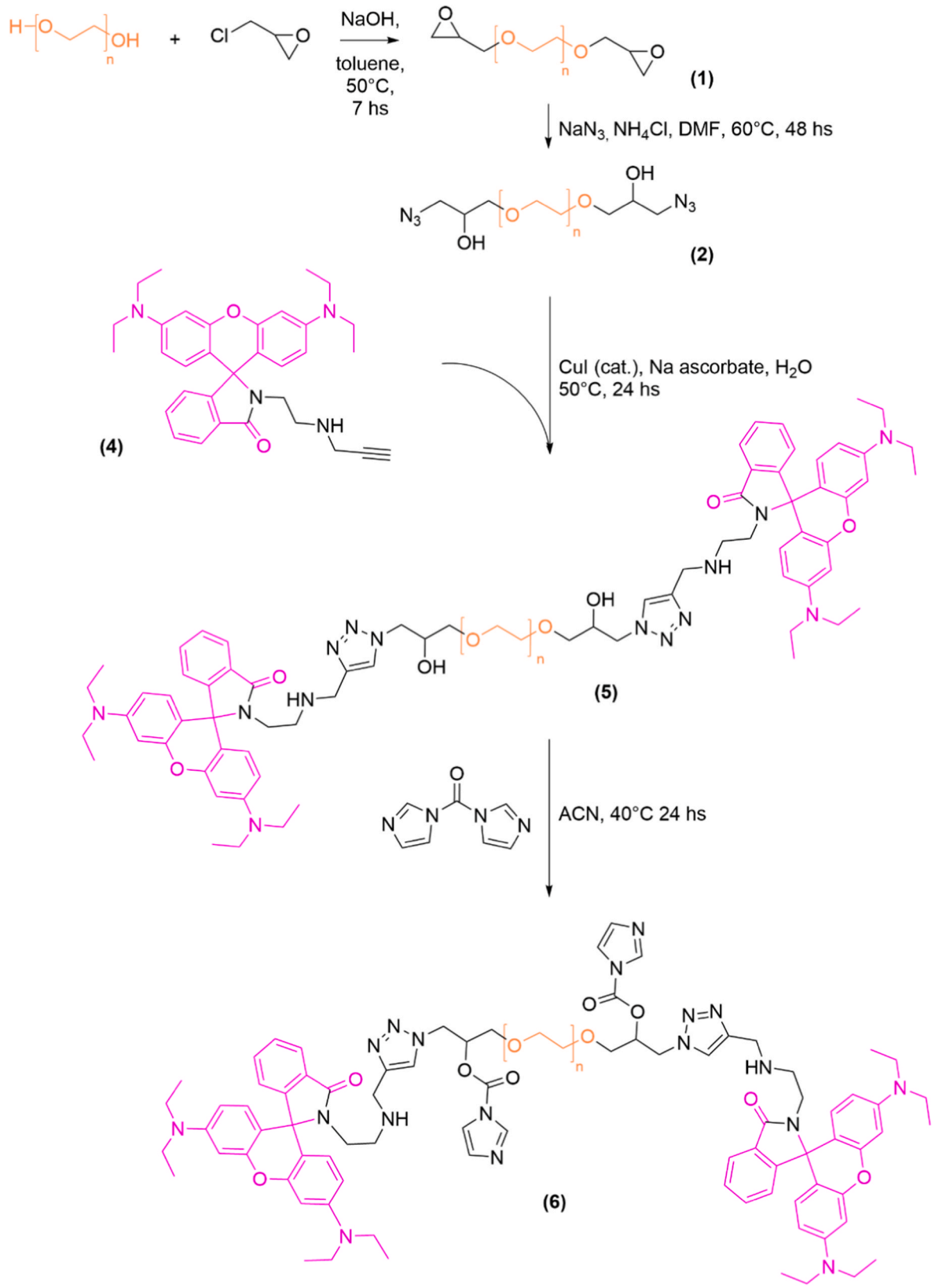

Scheme 2. Stepwise functionalization of PEG toward a fluorescent clickable macromer. PEG was first converted into diepoxy-PEG **(1)** via epichlorohydrin activation, followed by epoxide ring-opening with sodium azide to yield PEG-N_3 **(2)**. Propargyl RhB-EDA **(4)** was subsequently conjugated to PEG-N_3 **(2)** via CuAAC click chemistry, affording PEG-RhB 5. Finally, PEG-RhB **(5)** was activated with CDI to generate reactive imidazolyl carbamate groups suitable for further cross-linking reactions.

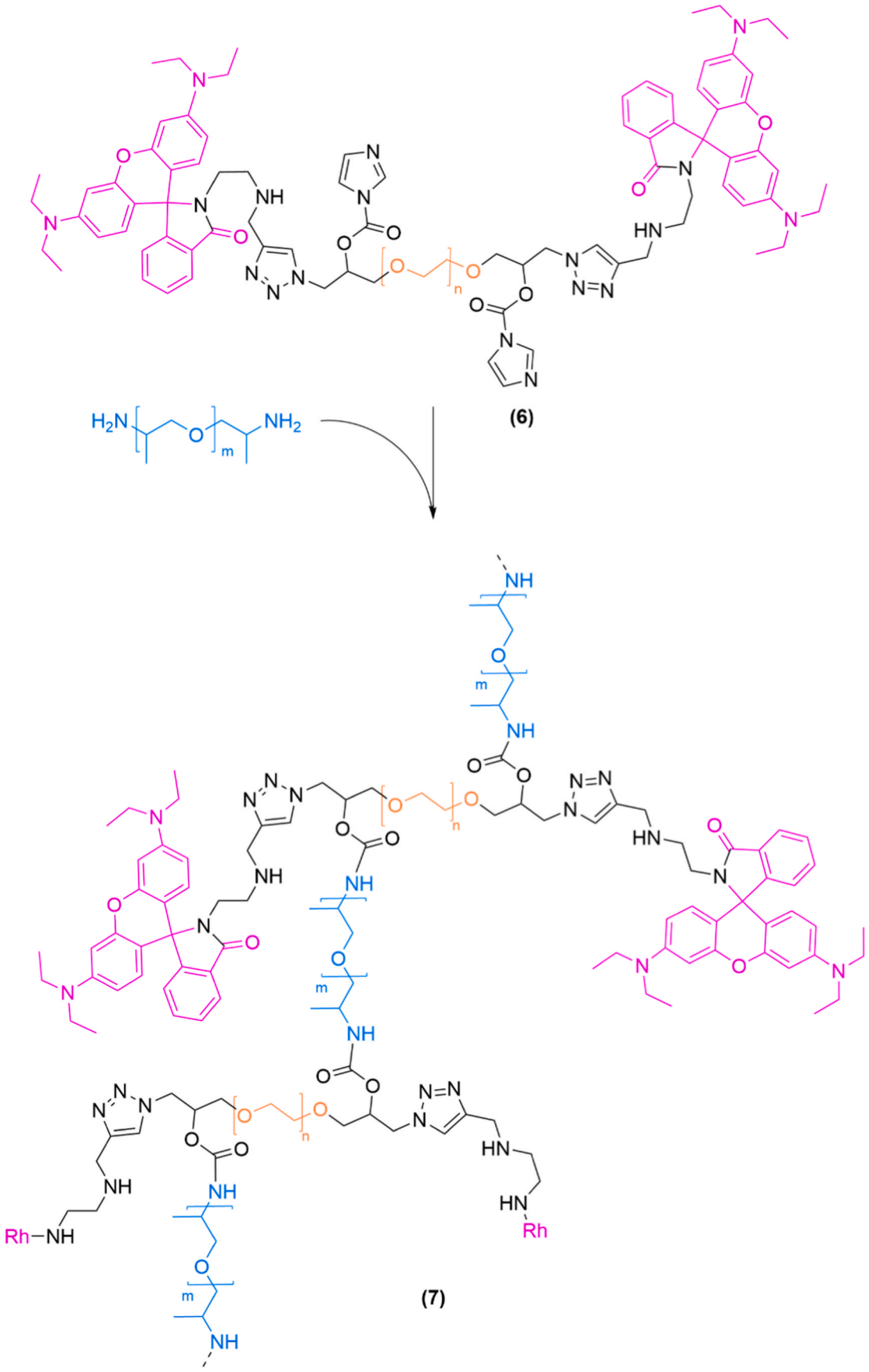

Scheme 3. Synthesis of PEG-Jeffamine nanogels via covalent crosslinking. PEG-CDI-RhB **(6)** was reacted with Jeffamine to form urethane-linked PEG-Jeffamine **(7)** networks through an emulsification-sonication-evaporation process.

stretching and the modification of the N–H region confirms the formation of R–O–C(O)–NH–R′ linkages within the nanogel network [50].

By employing gentle reaction conditions and an organic-aqueous biphasic medium, the local exposure of the rhodamine B core to harsh reagents is minimized, thereby preserving its conjugated structure and photophysical properties even through crosslinking [51]. Indeed, prior work on fluorescent labelling in polymer matrices has shown that careful control of crosslinking chemistry can maintain fluorophore stability and emission behavior. In our case, the successful incorporation and preservation of rhodamine B within the nanogel network were confirmed by both fluorescence microscopy and spectroscopic analysis. Fluorescence microscopy revealed a homogeneous fluorescent signal, while the emission maximum remained centered at 585 nm, consistent with that of free rhodamine B (Figs. S11 and S12). Control dialysis experiments further confirmed the stability of the covalently bound fluorophore, as no detectable rhodamine B release from the nanogel structure was observed over time. The resulting PEG-Jeffamine nanogels exhibited excellent dispersion stability, with an average hydrodynamic diameter of 95 ± 5 nm and a polydispersity index of 0.281, as determined by DLS measurements (Fig. S13). The average hydrodynamic diameter was determined to be 95 nm, indicating a consistent nanoscale size distribution suitable for biomedical applications. The PDI value of 0.281 reflects a relatively narrow size distribution, suggesting a well-defined nanoparticle population with minimal polydispersity. The stability of PEG-Jeffamine nanogels over time was assessed monitoring hydrodynamic diameter at predefined intervals until 2 weeks (Fig. S14). The results confirmed the colloidal stability of the nanogels throughout the observation period, with no significant signs of aggregation or destabilization. Furthermore, the initial zeta potential of −14 mV indicates moderate electrostatic stability (Fig. S15). Preliminary optimization experiments were performed by varying the equal flow rates of the two inlet streams from 100 to 4000 μL min^{-1} per channel, while maintaining a constant flow rate ratio of 1:1. Among the tested conditions, 1000/1000 μL min^{-1} provided the lowest polydispersity index and was therefore selected for all subsequent experiments. The polymer concentrations were not further varied in order to maintain the same precursor ratio used in the corresponding batch synthesis and ensure a consistent comparison between batch and flow conditions (Table S1).

When nanogels were instead fabricated under continuous-flow conditions, the resulting particles displayed a hydrodynamic diameter of 103 ± 5 nm and a PDI of 0.234 (Fig. S16). The slightly larger size yet lower polydispersity indicates that microfluidic synthesis enhanced mixing uniformity and controlled the nucleation-growth dynamics, leading to more homogeneous nanogel populations. The improved monodispersity likely stems from the rapid and reproducible interdiffusion of the polymer streams within the split-and-recombine (SAR) micromixer, which minimizes local concentration gradients and prevents secondary aggregation events. To broaden the potential applications of the nanogel system, surface functionalization with amine groups (-NH_2) was employed, enabling fine-tuning of the surface charge without altering the core physicochemical properties of the nanogel. This post-functionalization yielded zeta potentials of +12.89 mV and size of 112 nm (Figs. S17 and S18). While absolute zeta potentials above ±30 mV are typically associated with enhanced colloidal stability due to strong electrostatic repulsion, the observed negative and moderately positive values still provided sufficient dispersion stability [52]. This is likely due to the contribution of steric stabilization from the PEGylated polymer network, which plays a dominant role in maintaining colloidal integrity. The ability to modulate surface charge independently of the nanogel's structural and physicochemical characteristics presents a valuable advantage, particularly for biomedical applications where surface charge critically influences interactions with cells, proteins, and biological barriers. Maintaining colloidal stability while minimizing undesirable interactions highlights the versatility and tunability of the developed nanogel platform. Quantitative morphometric analysis was performed on cryo-TEM micrographs using ImageJ, considering several independent acquisitions for both batch (Fig. 2a) and flow (Fig. 2b) synthesized nanogels to ensure statistical representativeness. The PEG-Jeffamine nanogels produced via batch synthesis exhibited an average particle size of 110.1 nm and a mean circularity value of 0.48, whereas nanogels obtained under continuous-flow conditions showed a smaller average size of 99.2 nm together with a markedly higher circularity value of 0.85.

Circularity, as defined by ImageJ (with values ranging from 0 for highly elongated or irregular objects to 1 for a perfect circle), is widely used to assess nanoparticle shape regularity in electron microscopy analyses [53]. In this context, circularity values below approximately 0.6 are typically associated with irregular or weakly anisotropic morphologies, while values above 0.8 are generally indicative of highly spherical and homogeneous nanostructures. The significantly higher circularity observed for flow-synthesized nanogels therefore reflects a more regular and isotropic morphology compared to their batch counterparts. This difference can be attributed to the distinct network formation kinetics imposed by the two synthetic approaches. While batch emulsification relies on stochastic droplet formation and local concentration gradients, continuous-flow synthesis provides a more controlled and homogeneous mixing environment, which favors isotropic crosslinking and uniform network growth. Notably, the analysis was conducted on a comparable and significant number of cryo-TEM acquisitions for both batch (51 analysis) and flow (47 analysis) samples, supporting the robustness of the observed trends.

3.3. Quantification of free azide groups via EDS using a sulfur-based click probe

To quantify the residual azide groups that remain chemically accessible for further functionalization, EDS analysis was performed using a sulfur-containing click probe (*p*-toluenesulfonyl-propargylamine). The probe reacts selectively with azide groups via Cu(I)-catalyzed azide–alkyne cycloaddition (CuAAC), introducing a sulfur atom that can be readily detected by EDS. Since sulfur is absent in the native PEG structures, its signal provides a specific marker for azide groups that are effectively accessible to the click reaction (Scheme 4) [54].

Three PEG-based samples with different degrees of functionalization were analyzed, as summarized in Table 1.

PEG-N_3 (100% available azides): 1.57% sulfur (reference for maximal azide content); partially functionalized PEG-RhB (theoretically 50%, based on the stoichiometric equivalents used in the RhB conjugation step): 0.95% sulfur, indicating that 60.5% of azide sites remained free; fully functionalized PEG-RhB (theoretically 100%, corresponding to full conversion of azide groups according to reaction stoichiometry): 0.32% sulfur, indicating that 20.4% of azide sites remained unreacted. These results demonstrate that azide groups are consumed in a predictable manner upon fluorophore conjugation.

The non-linear decrease in sulfur signal between the theoretical 50% and 100% functionalization levels suggests that not all azide groups remain equally accessible as the degree of substitution increases. Although the present analysis does not allow a direct mechanistic determination, this behavior can be reasonably attributed to steric hindrance introduced by the bulky rhodamine B moieties and to local microenvironmental constraints within the polymeric structure [55].

As additional RhB groups are attached, neighboring azide sites may become partially shielded, reducing their accessibility during the click reaction [56]. Similar limitations in conversion have been reported in polymer functionalization and “grafting-onto” strategies, where steric congestion around reactive sites can hinder complete substitution in multi-functional macromolecular systems [57].

3.4. Drug release

The encapsulation performance of PEG-Jeffamine nanogels was

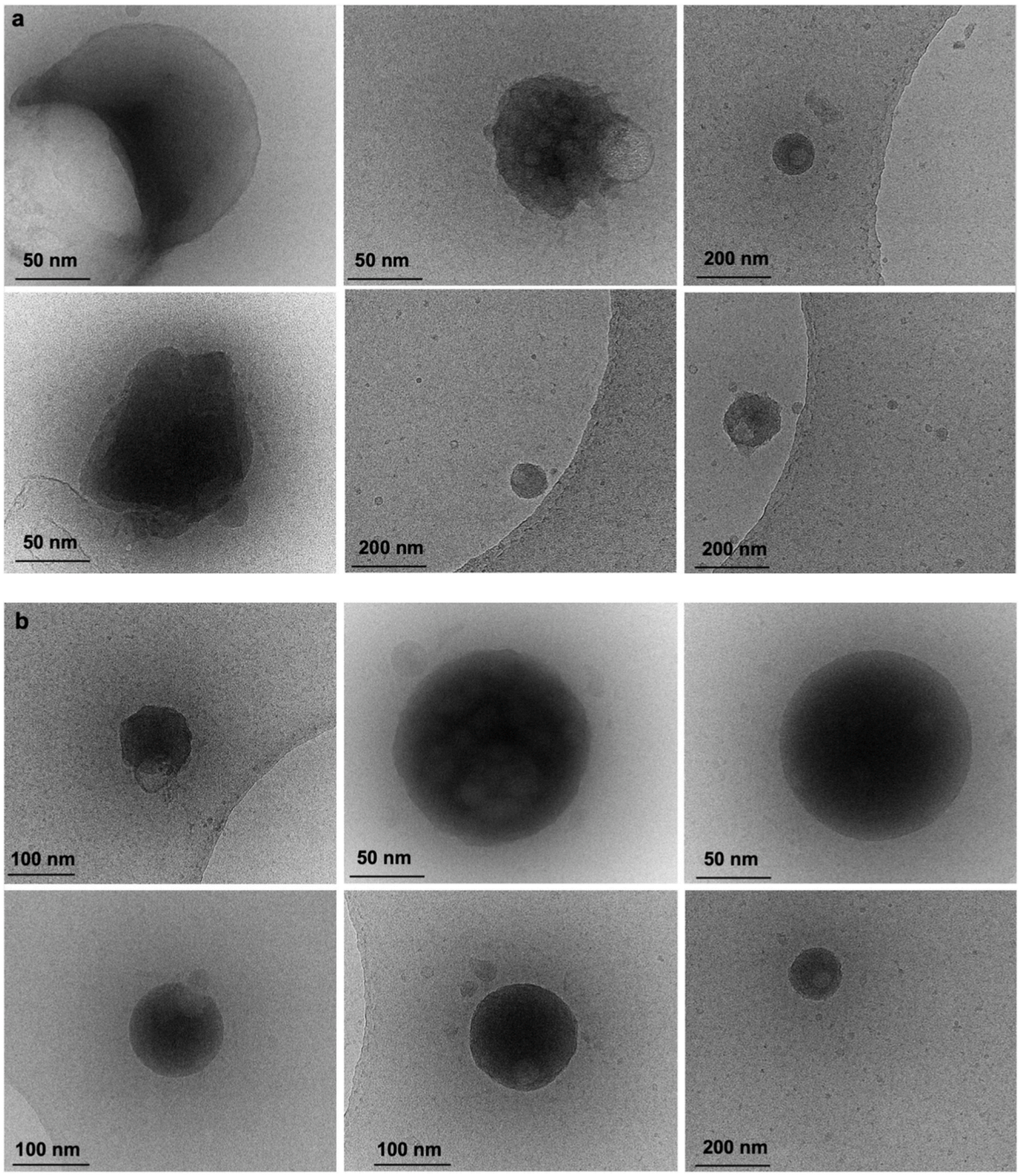

Fig. 2. Cryo-TEM images of PEG-Jeffamine nanogels synthesized by different preparation methods. (a) Nanogels obtained via batch emulsification-sonication-evaporation; (b) Nanogels synthesized under continuous-flow conditions.

systematically evaluated using two model molecules with contrasting hydrophilicity: FITC (hydrophobic) and RhB (hydrophilic). The dual-drug model allowed assessment of the platform's ability to accommodate molecules of different solubility profiles under both batch and microfluidic conditions [58–60]. The four configurations investigated (Batch/Batch, Flow/Batch, Batch/Flow, and Flow/Flow) correspond to different combinations of nanogel synthesis and drug-loading procedures rather than four distinct nanogel formulations. Although FITC contains a reactive isothiocyanate group that can react with free primary amines, the Jeffamine amines are largely consumed during CDI-mediated crosslinking with PEG, yielding carbamate (urethane) linkages within the nanogel network [61–63]. Consequently, the number of accessible primary amine groups is greatly reduced, and covalent conjugation between FITC and the polymer matrix is considered unlikely under the employed conditions [64]. The encapsulation of the model dyes can be described as a combination of diffusion-driven partitioning and physical entrapment within the polymer network during nanogel formation [3]. Rhodamine B, due to its relatively hydrophilic character, preferentially partitions within the PEG-rich aqueous domains of the nanogel matrix and can interact with the polymer chains through hydrogen bonding and electrostatic interactions [65]. In contrast, FITC exhibits lower aqueous solubility and shows stronger affinity for the relatively hydrophobic regions associated with the Jeffamine segments of the network [66]. Such encapsulation mechanisms, based on molecular partitioning and physical confinement within polymer meshes, are commonly observed in nanogel-based drug

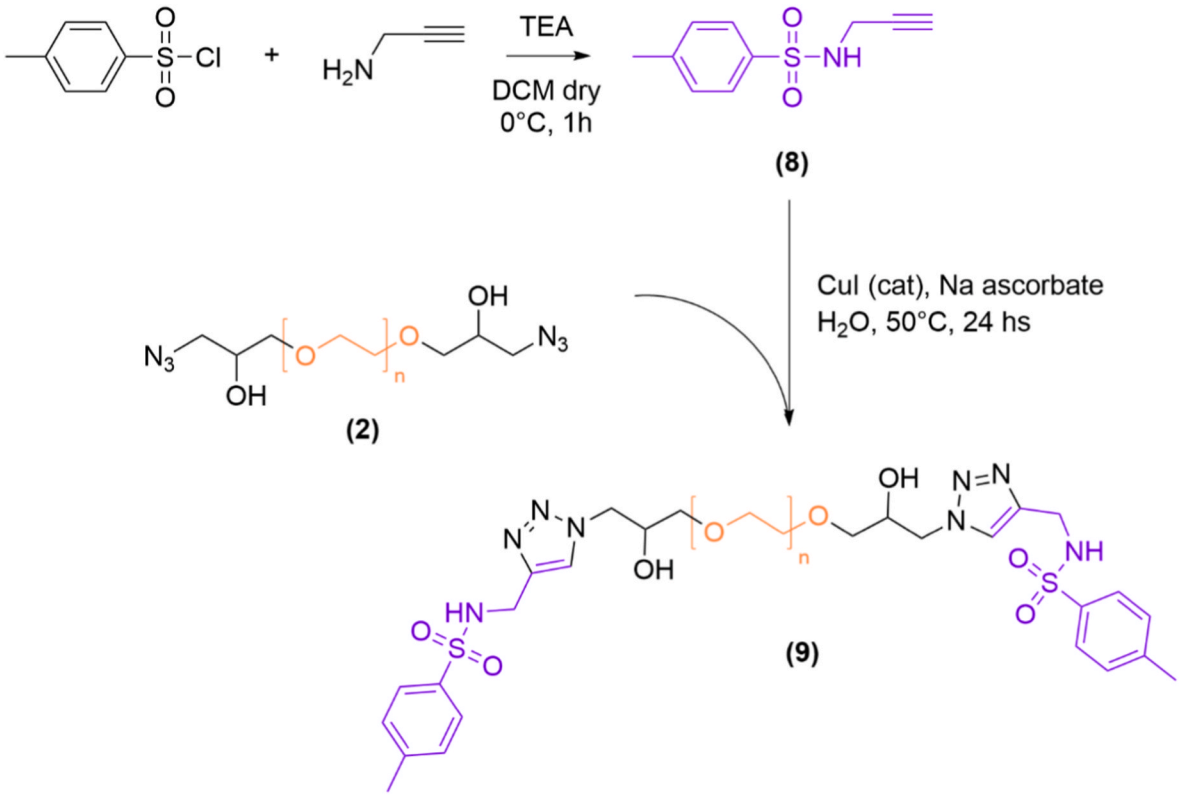

Scheme 4. Synthesis of the sulfur-containing probe and its conjugation to PEG-azide via CuAAC reaction. *p*-Toluenesulfonyl chloride reacts with propargylamine to afford the sulfonamide derivative **(8)**. Subsequently, compound **(8)** is conjugated to PEG-azide **(2)** via a Cu(I)-catalyzed azide–alkyne cycloaddition (CuAAC) in aqueous medium (CuI, sodium ascorbate) at 50 °C for 24 h, yielding the corresponding triazole-linked PEG derivative **(9)**.

Table 1
Quantification of residual azide groups in PEG-based systems using the sulfur-containing probe (*p*-toluenesulfonyl-propargylamine).

Sample	Nominal Functionalization	Sulfur Content (% S)	Estimated Free Azide Sites (% of total)	Interpretation
PEG-N_3	100 % available azide sites (reference)	1.57	100 %	Maximum azide content, used as calibration reference.
PEG-RhB (50%) partially functionalized	50 % of azide sites conjugated to RhB	0.95	60.5 %	Partial consumption of azide sites; majority of sites remain available for coupling.
PEG-RhB (100 %) fully functionalized	All azide sites targeted for conjugation	0.32	20.4 %	Incomplete conversion likely due to steric or microenvironmental effects.

delivery systems [16].

In the flow/flow configuration, the simultaneous mixing and crosslinking occurring within the microfluidic channels promote in situ entrapment of the dye molecules during network formation, which contributes to the higher encapsulation efficiencies observed compared to post-loading approaches. As shown in Table 2, a clear trend emerged across all formulations, with encapsulation efficiency (EE%) and drug loading (DL%) progressively increasing from conventional batch synthesis to fully continuous microfluidic synthesis. A complementary physicochemical characterization of all formulations, including hydrodynamic size and PDI, is reported in the Supporting Information (Table S2). Notably, the higher PDI values observed for drug-loaded systems are consistent with the presence of residual free dye and the known limitations of DLS in fluorescent systems [67].

Table 2
Comparison of FITC isomer I and RhB encapsulation efficiencies (EE%), drug loadings (DL%) and and cumulative release at 8 h (CR_8h, %) in PEG-Jeffamine nanogels synthesized via different batch and flow configurations.

Method	FITC-EE (%)	FITC-DL (%)	FITC-CR_8h (%)	RhB-EE (%)	RhB-DL (%)	RhB-CR_8h (%)
Batch/Batch	54.21 ± 3.76	2.64	65.77	92.11 ± 1.32	4.40	57.19
Flow/Batch	67.38 ± 1.25	3.26	59.16	93.45 ± 0.89	4.46	55.19
Batch/Flow	72.81 ± 2.02	3.51	47.27	95.02 ± 0.56	4.54	35.28
Flow/Flow	84.90 ± 1.42	4.07	20.1	95.92 ± 0.57	4.58	27.1

For FITC, EE% values increased from 54.2 % (batch/batch) to 84.9 % (flow/flow), while DL% improved from 2.64 % to 4.07 % under the same conditions. A similar enhancement was observed for rhodamine B, with EE% rising from 92.1 % (batch/batch) to 95.9 % (flow/flow) and DL% from 4.40 % to 4.58 %. These results demonstrate that the integration of microfluidic synthesis and encapsulation (flow/flow configuration) enables superior drug entrapment and reproducibility compared to traditional batch processes coupled with a scalable in-flow production.

The improvement can be attributed to the enhanced micromixing and rapid molecular diffusion achieved within the split-and-recombine (SAR) microfluidic channels, which ensure homogeneous distribution of both polymer and drug during crosslinking. This uniform reaction environment minimizes phase separation and diffusion losses that

typically occur in batch emulsification systems, particularly for hydrophobic compounds such as FITC. The higher encapsulation observed in flow-based systems also suggests that microfluidic confinement promotes more efficient network formation, likely resulting in tighter polymer meshes capable of retaining a greater fraction of the drug during the crosslink reaction. Furthermore, the mild, solvent-free aqueous environment preserved the chemical integrity of both dyes, confirming that the platform is suitable for encapsulating delicate fluorescent or bioactive molecules. The in vitro release profiles of RhB and FITC from PEG-Jeffamine nanogels at 37 °C in PBS (pH 7.4) are reported in Fig. 3. Both dyes exhibited a biphasic release pattern characterized by an initial burst phase followed by a sustained diffusion-controlled phase, whose magnitude and kinetics varied depending on the synthesis configuration. This is a common feature in matrix-based systems, where high water uptake and porosity facilitate the early diffusion of loosely associated molecules [68]. As this gradient diminishes, the release rate slows, consistent with diffusion-controlled release of RhB molecules retained within the polymer network. For rhodamine B (Fig. 3a), all formulations displayed a rapid initial release within the first 8 h (Table 2), corresponding to the desorption of surface-bound molecules and the diffusion of loosely entrapped species from the outer regions of the nanogel network. Interesting, the extent of the burst phase decreased progressively from batch/batch to flow/flow, indicating that microfluidic-assisted synthesis and loading significantly mitigated the initial release (Fig. 3c). This is well visible plotting the release percentage against the time $t^{1/2.3}$. As reported in literature, this mathematical model is representative of Fickian diffusion, and the y-axis intercept value is an indication of the percentage of burst release: an ideal controlled drug delivery system should present linear trend and the y-axis intercept equal to zero [69].

The slower and more gradual release observed in the flow-processed nanogels is consistent with a more homogeneous polymer network, as also suggested by the narrower size distribution (PDI ≈ 0.23) and higher encapsulation efficiency (EE ≈ 96 %). The controlled mass transfer achieved within the split-and-recombine micromixer during synthesis likely promotes more uniform crosslinking, which can reduce the presence of loosely associated drug molecules at the nanogel surface and consequently limit the initial burst release. This interpretation is also supported by the structural characterization of the nanogels. DLS measurements indicated a relatively narrow size distribution, while TEM images revealed well-defined spherical particles with homogeneous morphology. Such structural features are typically associated with more uniform polymer networks, which can enhance drug confinement within the nanogel matrix and reduce premature diffusion of loosely associated molecules. Similar relationships between particle morphology, size distribution, and encapsulation performance have been reported in previous studies on nanogel-based drug delivery systems [38,70–72]. In contrast, FITC-loaded nanogels (Fig. 3b) exhibited an overall lower cumulative release, reflecting the dye's lower aqueous solubility and stronger hydrophobic interactions within the Jeffamine-rich domains of the network. Here too, the transition from batch to flow configurations markedly influenced the release profile. The batch/batch sample appeared to release a higher fraction; however, this apparent increase stems from its lower initial loading (DL = 2.64 %), meaning that the absolute amount of released FITC was in fact smaller than in the flow-based systems. As the encapsulation efficiency improved (up to 84.9 % and DL = 4.07 % in the flow/flow mode), the release curves became more gradual, with a reduced burst and a more sustained trend over 24 h (Fig. 3d). This behavior indicates that the enhanced encapsulation achieved under microfluidic conditions also translated into

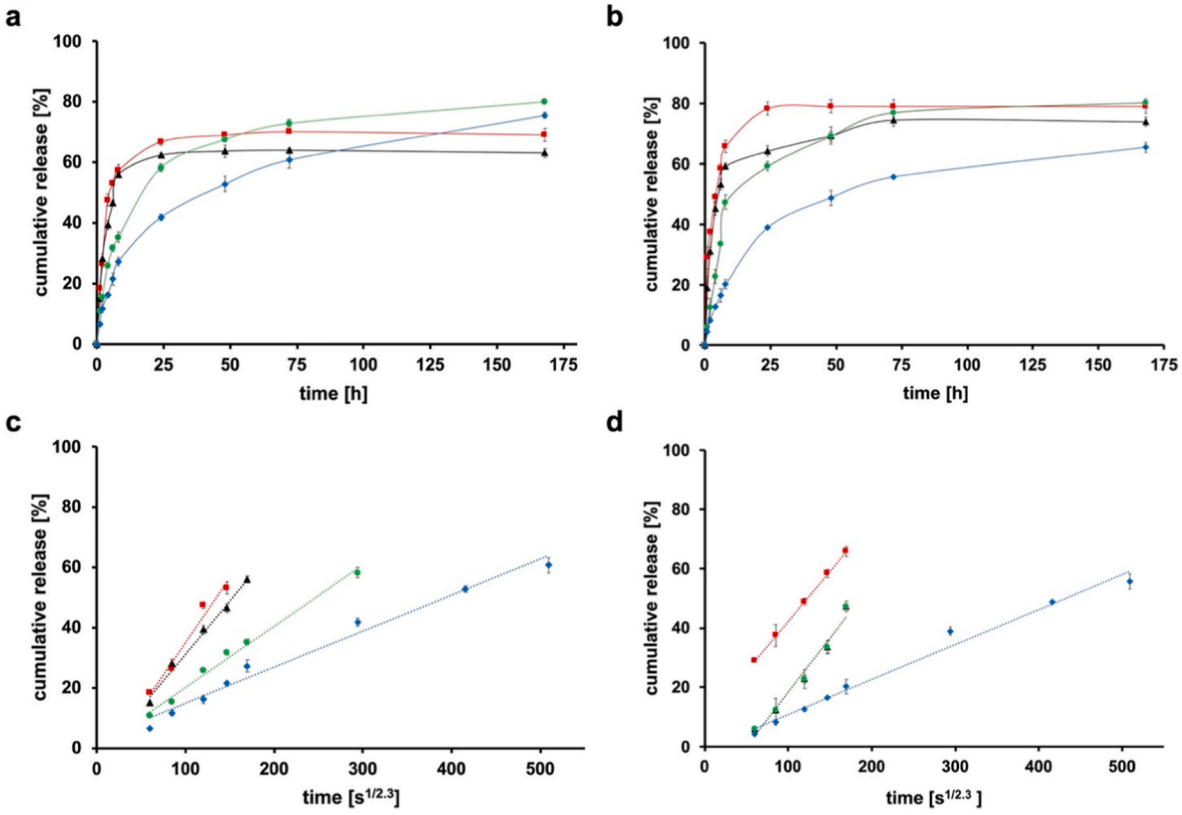

Fig. 3. a) The in vitro cumulative release profiles of RhB from PEG-Jeffamine NGs prepared using different synthesis and loading configurations: Batch/Batch (red), Flow/Batch (black), Batch/Flow (green), and Flow/Flow (blue); b) The in vitro cumulative release profiles of FITC from PEG-Jeffamine nanogels prepared using different synthesis and loading configurations: Batch/Batch (red), Flow/Batch (black), Batch/Flow (green), and Flow/Flow (blue); c, d) The slope of the RhB and FITC release against the variable time expressed at $t^{1/2.3}$ is representative of the Fickian diffusion coefficient of the drug in NGs Release studies were conducted in PBS (pH 7.4) at 37 °C under sink conditions. Data (n = 3) are expressed as mean ± SD.

stronger retention and slower diffusion of the probe within the polymeric network. Overall, both model compounds confirmed that integrating microfluidics into the nanogel synthesis and loading process produces denser and more homogeneous structures, capable of moderating the initial burst while maintaining continuous, diffusion-governed release.

The flow/flow configuration offered the best balance between encapsulation efficiency and controlled release for both hydrophilic (RhB) and hydrophobic (FITC) molecules, demonstrating the versatility of this approach for designing tunable nanogel-based delivery systems.

3.5. Cytotoxicity evaluation of PEG-Jeffamine nanogels via LDH assay

The cytotoxicity of PEG-Jeffamine nanogels was evaluated by the lactate dehydrogenase (LDH) assay, which quantifies membrane integrity loss as an indicator of cytotoxic stress.

Primary mixed spinal cord cultures were used, as they represent a physiologically relevant in vitro model, allowing the evaluation of nanogel effects across multiple neural cell types with different vulnerability profiles. Mixed cultures are particularly advantageous for biocompatibility studies because they better recapitulate the cellular complexity of the central nervous system compared to immortalized or cancer-derived cell lines, which, despite their unlimited proliferation capacity, often differ biologically from normal cells [73,74]. Indeed, primary mixed neural cultures more closely mimic the in vivo cellular environment and provide biologically relevant data [75,76]. This experiment was designed as a preliminary evaluation of the cytocompatibility of PEG-Jeffamine nanogels, providing an initial indication of their suitability for biomedical applications. As shown in Fig. 4, untreated control cells (CTRL) and LPS-stimulated cultures (LPS) exhibited negligible LDH release, confirming minimal baseline cytotoxicity under the experimental conditions. Treatment with PEG-Jeffamine nanogels at dilutions of 1:500 resulted in LDH levels comparable to those observed in control groups, confirming good biocompatibility at this concentration. Importantly, although an increasing trend in LDH release was observed at the highest concentration (1:50), the overall LDH levels remained limited, indicating that PEG-Jeffamine nanogels are largely tolerated by mixed spinal cord cultures even at elevated concentrations. Consistent with literature reports indicating increased sensitivity of primary neural cells to high concentrations of cross-linked nanogels [77–79], these results support the presence of a broad biocompatibility window for PEG-Jeffamine nanogels, in which increasing concentrations remain overall compatible with the culture, with only selective effects on the most fragile neural populations. Overall, these data highlight the favourable cytocompatibility profile of PEG-Jeffamine nanogels, reinforcing their suitability for applications requiring prolonged exposure or relatively high dosing.

4. Conclusions

In this work, we established a fully aqueous and scalable microfluidic approach for the synthesis of PEG-Jeffammine nanogels, enabling a level of control that is difficult to achieve through conventional batch emulsification. By comparing four fabrication/loading configurations, we demonstrated that continuous-flow synthesis coupled with in-line drug loading (flow/flow) yields nanogels with superior encapsulation efficiency, reduced burst release, and a more homogeneous internal architecture. Structural analyses confirmed the formation of well-defined, monodisperse nanogels, while the preservation of residual azide groups provides a modular handle for future functionalization. Importantly, PEG-Jeffamine nanogels exhibited excellent biocompatibility in primary mixed spinal cord cultures, with overall LDH levels remaining low even at elevated concentrations, and only the more vulnerable cell populations, showing early signs of sensitivity. Overall, this study highlights how combining Jeffamine chemistry with microfluidic engineering offers a robust and versatile platform for producing advanced nanogels, paving the way for more precise, reproducible, and clinically translatable nanoscale drug delivery systems.

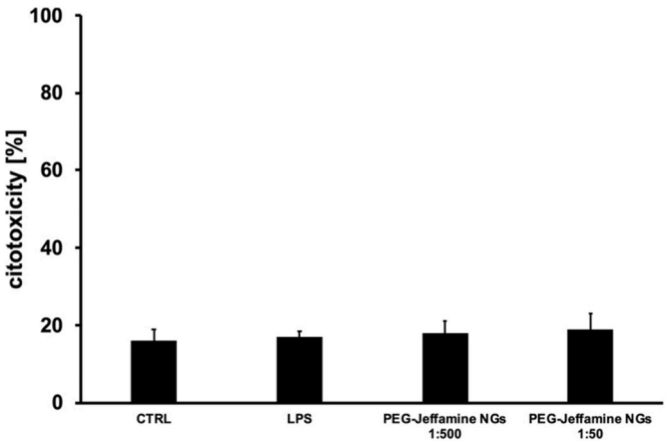

Fig. 4. LDH cytotoxicity assay comparing PEG-Jeffamine nanogels at different dilutions.

CRediT authorship contribution statement

Giuseppe Nunziata: Writing – original draft, Methodology, Investigation. **Fabio Pizzetti:** Writing – review & editing, Methodology. **Valeria Veneruso:** Methodology. **Arianna Rossetti:** Writing – review & editing, Methodology. **Emilia Petillo:** Methodology. **Enrico Frigerio:** Methodology. **Chiara Marabelli:** Methodology. **Mattia Tiboni:** Methodology. **Luca Casettari:** Methodology. **Pietro Veglianese:** Writing – review & editing, Methodology. **Alessandro Sacchetti:** Writing – review & editing, Methodology. **Filippo Rossi:** Writing – review & editing, Resources, Project administration.

Declaration of competing interest

The authors declare that they have no known competing financial interests or personal relationships that could have appeared to influence the work reported in this paper.

Appendix A. Supplementary data

Supplementary data to this article can be found online at https://doi.org/10.1016/j.mtchem.2026.103587.

Data availability

Data will be made available on request.

References

[1] A. Bharadwaj, M. Gupta, M. Verma, P. Gangwar, N. Wahi, Advancements of nanobiotechnology in public health sector: benefits and challenges, Nanosci. Nanotechnol. - Asia 14 (2024) E22106812316402, https://doi.org/10.2174/0122106812316402240808101033.
[2] X. Wang, H. Li, C. Chen, Z. Liang, Understanding of endo/lysosomal escape of nanomaterials in biomedical application, Smart Molecul. (2025) e20240017.
[3] R.T. Chacko, J. Ventura, J. Zhuang, S. Thayumanavan, Polymer nanogels: a versatile nanoscopic drug delivery platform, Adv. Drug Deliv. Rev. 64 (2012) 836–851, https://doi.org/10.1016/j.addr.2012.02.002.
[4] L. Arnfast, C.G. Madsen, L. Jorgensen, S. Baldursdottir, Design and processing of nanogels as delivery systems for peptides and proteins, Ther. Deliv. 5 (2014) 691–708, https://doi.org/10.4155/tde.14.38.
[5] G. Nunziata, D. Pollonio, E. Lacroce, F. Rossi, Smart pH-Responsive polymers in biomedical applications: nanoparticles, hydrogels, and emerging hybrid platforms, Mater. Today Chem. 49 (2025) 103063.
[6] S. Xie, L. Wei, Y. Liu, J. Meng, W. Cao, B. Qiu, X. Li, Size-tunable nanogels for cascaded release of metronidazole and chemotherapeutic agents to combat fusobacterium nucleatum-infected colorectal cancer, J. Contr. Release 365 (2024) 16–28.

[7] A.A. Ali, A. Al-Othman, M.H. Al-Sayah, Multifunctional stimuli-responsive hybrid nanogels for cancer therapy: current status and challenges, J. Contr. Release 351 (2022) 476–503, https://doi.org/10.1016/j.jconrel.2022.09.033.

[8] R. Kandil, O.M. Merkel, Recent progress of polymeric nanogels for gene delivery, Curr. Opin. Colloid Interface Sci. 39 (2019) 11–23, https://doi.org/10.1016/j.cocis.2019.01.005.

[9] S.A. Ferreira, F.M. Gama, M. Vilanova, Polymeric nanogels as vaccine delivery systems, Nanomed. Nanotechnol. Biol. Med. 9 (2013) 159–173, https://doi.org/10.1016/j.nano.2012.06.001.

[10] G. Nunziata, F. Pizzetti, P. Veglianese, G. Forloni, C. Balducci, F. Rossi, Can nanoparticle-based intranasal delivery systems revolutionize treatment of central nervous system diseases? Expet Opin. Drug Deliv. 23 (2025) 7–11.

[11] Y. Yin, B. Hu, X. Yuan, L. Cai, H. Gao, Q. Yang, Nanogel: a versatile nano-delivery system for biomedical applications, Pharmaceutics 12 (2020) 290, https://doi.org/10.3390/pharmaceutics12030290.

[12] G. Nunziata, E. Limiti, D. Aramini, M. Nava, L. Moretti, A. Rainer, M. Sponchioni, F. Rossi, pH-Thermo dual-responsive polymeric nanoparticles for women's health: dual action against cervical and ovarian cancer cells, ACS Appl. Mater. Interfaces 17 (2025) 61888–61904.

[13] E. Lacroce, F. Pizzetti, N.M.B. Urrego, G. Nunziata, M. Masi, F. Rossi, Magnetically active bicontinuous polymer structures for multiple controlled drug delivery, Macromol. Biosci. 24 (2024) 2400084.

[14] Y.E. Karaçoban, N. Işıklan, Design, development, and characterization of pH-responsive chitosan-graft-poly(2-(diethylamino)ethyl acrylamide/acrylic acid) copolymeric nanogels for controlled and sustained erlotinib release, Mater. Today Chem. 52 (2026) 103345, https://doi.org/10.1016/j.mtchem.2026.103345.

[15] Y. Zou, D. Li, M. Shen, X. Shi, Polyethylenimine-based nanogels for biomedical applications, Macromol. Biosci. 19 (2019) 1900272, https://doi.org/10.1002/mabi.201900272.

[16] A.V. Kabanov, S.V. Vinogradov, Nanogels as pharmaceutical carriers: finite networks of infinite capabilities, Angew. Chem. Int. Ed. 48 (2009) 5418–5429.

[17] H. Zhang, Q. Li, Y. Zhang, Y. Xia, L. Yun, Q. Zhang, T. Zhang, X. Chen, H. Chen, W. Li, A nanogel with passive targeting function and adjustable polyplex surface properties for efficient anti-tumor gene therapy, RSC Adv. 6 (2016) 84445–84456, https://doi.org/10.1039/C6RA13707E.

[18] S. Wen, F. Zheng, M. Shen, X. Shi, Surface modification and PEGylation of branched polyethyleneimine for improved biocompatibility, J. Appl. Polym. Sci. 128 (2013) 3807–3813, https://doi.org/10.1002/app.38444.

[19] M. Khansarizadeh, A. Mokhtarzadeh, M. Rashedinia, S. Taghdisi, P. Lari, K. Abnous, M. Ramezani, Identification of possible cytotoxicity mechanism of polyethylenimine by proteomics analysis, Hum. Exp. Toxicol. 35 (2016) 377–387, https://doi.org/10.1177/0960327115591371.

[20] E. Wagner, J. Kloeckner, Gene delivery using polymer therapeutics, in: R. Satchi-Fainaro, R. Duncan (Eds.), Polymer Therapeutics I, Springer, Berlin, Heidelberg, 2006, pp. 135–173, https://doi.org/10.1007/12_023.

[21] J. Casper, S.H. Schenk, E. Parhizkar, P. Detampel, A. Dehshahri, J. Huwyler, Polyethylenimine (PEI) in gene therapy: current status and clinical applications, J. Contr. Release 362 (2023) 667–691, https://doi.org/10.1016/j.jconrel.2023.09.001.

[22] N. Mohammadi, N. Fayazi Hosseini, H. Nemati, H. Moradi-Sardareh, M. Nabi-Afjadi, G.A. Kardar, Revisiting of properties and modified polyethylenimine-based cancer gene delivery systems, Biochem. Genet. 62 (2024) 18–39, https://doi.org/10.1007/s10528-023-10416-7.

[23] M. Wang, Y. Sun, M. Wang, Z. Yang, Y. Shi, D. Zeng, L. Liu, Enhancing the safety and effectiveness of polyethylenimine gene delivery through cell membrane encapsulation, J. Drug Deliv. Sci. Technol. 92 (2024) 105376, https://doi.org/10.1016/j.jddst.2024.105376.

[24] R. Yu, Nouveaux Hydrogels À Liaison imine double préparés à partir d'O-carboxyméthyl chitosane et de Jeffamine par chimie covalente dynamique pour applications biomédicales, phdthesis, Université Montpellier, 2021. https://theses.hal.science/tel-03346833. (Accessed 24 February 2025).

[25] F. Pinelli, M. Saadati, A. Rossetti, F. Rossi, A. Sacchetti, On the influence of polyethyleneimine modification in nanogel-driven drug delivery, Colloids Surf. A Physicochem. Eng. Asp. 658 (2023) 130623.

[26] L. Castan, C. José da Silva, E. Ferreira Molina, R. Alves Dos Santos, Comparative study of cytotoxicity and genotoxicity of commercial Jeffamines® and polyethylenimine in CHO-K1 cells, J. Biomed. Mater. Res. B Appl. Biomater. 106 (2018) 742–750, https://doi.org/10.1002/jbm.b.33882.

[27] H.V. Le, V. Dulong, L. Picton, D. Le Cerf, Lyophilization for formulation optimization of drug-loaded thermoresponsive polyelectrolyte complex nanogels from functionalized hyaluronic acid, Pharmaceutics 15 (2023), https://doi.org/10.3390/pharmaceutics15030929.

[28] S. Akar, S. Fardindoost, M. Hoorfar, High throughput microfluidics-based synthesis of PEGylated liposomes for precise size control and efficient drug encapsulation, Colloids Surf. B Biointerfaces 238 (2024) 113926, https://doi.org/10.1016/j.colsurfb.2024.113926.

[29] F. Yao, J. Wang, W. Zhang, Z. Wang, Y. Li, H. Sun, Q. Chen, P. Liang, A microfluidic platform for minute-scale synthesizing Au@Ag nanocubes, Mater. Today Chem. 34 (2023) 101825, https://doi.org/10.1016/j.mtchem.2023.101825.

[30] E. Lallana, R. Donno, D. Magri, K. Barker, Z. Nazir, K. Treacher, M.J. Lawrence, M. Ashford, N. Tirelli, Microfluidic-assisted nanoprecipitation of (PEGylated) poly (D, L-lactic acid-co-caprolactone): effect of macromolecular and microfluidic parameters on particle size and paclitaxel encapsulation, Int. J. Pharm. 548 (2018) 530.

[31] G. Nunziata, M. Nava, E. Lacroce, F. Pizzetti, F. Rossi, Thermo-responsive polymer-based nanoparticles: from chemical design to advanced applications, Macromol. Rapid Commun. (2025) 2401127.

[32] D. Tomioka, S.A. Jung, A. Pich, M. Matsusaki, Fabrication of oxygen-releasing dextran microgels by droplet-based microfluidic method, RSC Adv. 14 (2024) 26544–26555.

[33] S. Roy, R. Kumar, A. Acooli, S. Roy, A. Chatterjee, S. Chattaraj, J. Nayak, B.-H. Jeon, A. Basu, S. Banerjee, Transforming nanomaterial synthesis through advanced microfluidic approaches: a review on accessing unrestricted possibilities, J. Compos. Sci. 8 (2024) 386.

[34] M. Besanjideh, M. Rezaeian, Z. Mahmoudi, A. Shamloo, S.K. Hannani, Investigating the effects of precursor concentration and gelling parameters on droplet-based generation of Ca-Alginate microgels: identifying new stable modes of droplet formation, Mater. Today Chem. 24 (2022) 100821, https://doi.org/10.1016/j.mtchem.2022.100821.

[35] L. Ma, X. Zhao, J. Hou, L. Huang, Y. Yao, Z. Ding, J. Wei, N. Hao, Droplet microfluidic devices: working principles, fabrication methods, and scale-up applications, Small Methods 8 (2024) 2301406.

[36] M. Dacos, B. Immordino, E. Diroff, G. Sicard, A. Kosta, A. Rodallec, S. Giacometti, J. Ciccolini, R. Fanciullino, Pegylated liposome encapsulating docetaxel using microfluidic mixing technique: process optimization and results in breast cancer models, Int. J. Pharm. 656 (2024) 124091, https://doi.org/10.1016/j.ijpharm.2024.124091.

[37] R. Krzysztoń, B. Salem, D. Lee, G. Schwake, E. Wagner, J.O. Rädler, Microfluidic self-assembly of folate-targeted monomolecular siRNA-lipid nanoparticles, Nanoscale 9 (2017) 7442–7453.

[38] Z. Whiteley, H.M.K. Ho, Y.X. Gan, L. Panariello, G. Gkogkos, A. Gavriilidis, D.Q. M. Craig, Microfluidic synthesis of protein-loaded nanogels in a coaxial flow reactor using a design of experiments approach, ††Electronic supplementary information (ESI) available. See DOI: 10.1039/d0na01051k, Nanoscale Adv. 3 (2021) 2039–2055, https://doi.org/10.1039/d0na01051k.

[39] P. Sacco, S. Pedroso-Santana, Y. Kumar, N. Joly, P. Martin, P. Bocchetta, Ionotropic gelation of chitosan flat structures and potential applications, Molecules 26 (2021) 660.

[40] S. Mandal, A. Sahana, A. Banerjee, D.A. Safin, M.G. Babashkina, K. Robeyns, S. Verkaart, J.G.J. Hoenderop, M.P. Mitoraj, Y. Garcia, D. Das, A smart rhodamine–pyridine conjugate for bioimaging of thiocyanate in living cells, RSC Adv. 5 (2015) 103350–103357, https://doi.org/10.1039/C5RA21838A.

[41] E. Mauri, P. Veglianese, S. Papa, A. Mariani, M. De Paola, R. Rigamonti, G.M. F. Chincarini, I. Vismara, S. Rimondo, A. Sacchetti, F. Rossi, Double conjugated nanogels for selective intracellular drug delivery, RSC Adv. 7 (2017) 30345–30356, https://doi.org/10.1039/C7RA04584K.

[42] M. Tiboni, M. Tiboni, A. Pierro, M.D. Papa, S. Sparaventi, M. Cespi, L. Casettari, Microfluidics for nanomedicines manufacturing: an affordable and low-cost 3D printing approach, Int. J. Pharm. 599 (2021) 120464, https://doi.org/10.1016/j.ijpharm.2021.120464.

[43] E. Lacroce, G. Nunziata, F. Cianniello, E. Limiti, A. Rainer, F.B. Vangosa, A. Sacchetti, M. Sponchioni, F. Rossi, Amphiphilic pH-responsive core-shell nanoparticles can increase the performances of cellulose-based drug delivery systems, Int. J. Biol. Macromol. (2024) 137659, https://doi.org/10.1016/j.ijbiomac.2024.137659.

[44] A. Rahdar, M. Almasi-Kashi, Photophysics of rhodamine B in the nanosized water droplets: a concentration dependence study, J. Mol. Liq. 220 (2016) 395–403, https://doi.org/10.1016/j.molliq.2016.05.002.

[45] M. Beija, C.A.M. Afonso, J.M.G. Martinho, Synthesis and applications of Rhodamine derivatives as fluorescent probes, Chem. Soc. Rev. 38 (2009) 2410–2433, https://doi.org/10.1039/B901612K.

[46] Y. Yao, J. Xue, M. Wang, D. Fu, Y. Shen, Y. Xue, F. Zhang, P. Liu, H. Wang, H. Wu, Tunable photoluminescent, water-resistant and flexible films prepared using hollow cellulose-based microspheres encapsulating hydrophobic fluorescent dyes, Chem. Eng. J. 482 (2024) 149116.

[47] F. Bauer, E. Schamel, H. Schlachter, G. Wehnert, D. Söthje, Bio-based epoxy resins from estragole: achieving high glass transition temperatures comparable to DGEBA and simultaneously low viscosities, Macromol. Mater. Eng. (2025) e00418.

[48] F. Pinelli, F. Pizzetti, Ó.F. Ortolà, A. Marchetti, A. Rossetti, A. Sacchetti, F. Rossi, Influence of the core formulation on features and drug delivery ability of carbamate-based nanogels, Int. J. Mol. Sci. 21 (2020) 6621, https://doi.org/10.3390/ijms21186621.

[49] G. Nunziata, A. Borroni, F. Rossi, Advanced microfluidic strategies for core-shell nanoparticles: the next-generation of polymeric and lipid-based drug nanocarriers, Chem. Eng. J. Adv. 22 (2025) 100759, https://doi.org/10.1016/j.ceja.2025.100759.

[50] B. Smith, The Infrared Spectra of Polymers, VI: Polymers with CO Bonds, 2022.

[51] S. Bou, A.S. Klymchenko, M. Collot, Fluorescent labeling of biocompatible block copolymers: synthetic strategies and applications in bioimaging, Mater. Adv. 2 (2021) 3213–3233.

[52] A. Olfati, N. Karimi, E. Arkan, M. Zhaleh, M. Mozafari, Enhancing bioavailability and stability of plant secondary metabolites: formulation and characterization of nanophytosomes encapsulating red bryony and horned poppy extracts, J. Funct. Biomater. 16 (2025) 194.

[53] R.I. Rs, Automated analysis of TiO 2 nanoparticles using deep learning in EM images: a review, IEEE (2024) 178–183.

[54] P.J. Weldrick, S. San, V.N. Paunov, Advanced alcalase-coated clindamycin-loaded carbopol nanogels for removal of persistent bacterial biofilms, ACS Appl. Nano Mater. 4 (2021) 1187–1201, https://doi.org/10.1021/acsanm.0c02810.

[55] N.C. Cabrera-Quiñones, L.J. López-Méndez, C. Cruz-Hernández, P. Guadarrama, Click chemistry as an efficient toolbox for coupling sterically hindered molecular systems to obtain advanced materials for nanomedicine, Int. J. Mol. Sci. 26 (2025), https://doi.org/10.3390/ijms26010036.
[56] S. Wang, X. Yang, W. Zhu, L. Zou, K. Zhang, Y. Chen, F. Xi, Strain-promoted azide-alkyne cycloaddition "click" as a conjugation tool for building topological polymers, Polymer 55 (2014) 4812–4819, https://doi.org/10.1016/j.polymer.2014.08.003.
[57] D. Makharadze, L.J. del Valle, R. Katsarava, J. Puiggalí, The art of PEGylation: from simple polymer to sophisticated drug delivery system, Int. J. Mol. Sci. 26 (2025), https://doi.org/10.3390/ijms26073102.
[58] S. Slomkowski, M. Gadzinowski, S. Sosnowski, I. Radomska-Galant, A. Pucci, C. De Vita, F. Ciardelli, Nanoparticles from polylactide and polyether block copolymers: formation, properties, encapsulation, and release of pyrene—Fluorescent model of hydrophobic drug, J. Nanosci. Nanotechnol. 6 (2006) 3242–3251.
[59] H. Chen, Y. Gu, Y. Hu, Comparison of two polymeric carrier formulations for controlled release of hydrophilic and hydrophobic drugs, J. Mater. Sci. Mater. Med. 19 (2008) 651–658.
[60] R. Zhang, M. Hummelgård, G. Lv, H. Olin, Real time monitoring of the drug release of rhodamine B on graphene oxide, Carbon 49 (2011) 1126–1132.
[61] G.T. Hermanson, Chapter 10 - fluorescent probes, in: G.T. Hermanson (Ed.), Bioconjugate Techniques, third ed.), third ed., Academic Press, Boston, 2013, pp. 395–463, https://doi.org/10.1016/B978-0-12-382239-0.00010-8.
[62] A.R. Morales, K.J. Schafer-Hales, A.I. Marcus, K.D. Belfield, Amine-reactive fluorene probes: synthesis, optical characterization, bioconjugation, and two-photon fluorescence imaging, Bioconjug. Chem. 19 (2008) 2559–2567, https://doi.org/10.1021/bc800415t.
[63] A. Tantipanjaporn, M.-K. Wong, Development and recent advances in lysine and N-Terminal bioconjugation for peptides and proteins, Molecules 28 (2023), https://doi.org/10.3390/molecules28031083.
[64] J. DeRuiter, Amides and related functional groups, Principles of Drug Action 1 (2005) 1–16.
[65] A. Pourjavadi, Z. Mazaheri Tehrani, R. Heydarpour, Z. Masihzadeh, Rhodamine-based fluorescent nanogel: a dual temperature and pH sensor, Sens. Imaging 24 (2023) 37.
[66] A. Hoffmann, J. Bredno, M. Wendland, N. Derugin, P. Ohara, M. Wintermark, High and low molecular weight fluorescein isothiocyanate (FITC)–Dextrans to assess blood-brain barrier disruption: technical considerations, Trans. Stroke Res. 2 (2011) 106–111.
[67] D. Geißler, C. Gollwitzer, A. Sikora, C. Minelli, M. Krumrey, U. Resch-Genger, Effect of fluorescent staining on size measurements of polymeric nanoparticles using DLS and SAXS, Anal. Methods 7 (2015) 9785–9790, https://doi.org/10.1039/C5AY02005K.
[68] J.P. Tan, Q. Wang, K.C. Tam, Control of burst release from nanogels via layer by layer assembly, J. Contr. Release 128 (2008) 248–254.
[69] P.L. Ritger, N.A. Peppas, A simple equation for description of solute release I. Fickian and non-fickian release from non-swellable devices in the form of slabs, spheres, cylinders or discs, J. Contr. Release 5 (1987) 23–36, https://doi.org/10.1016/0168-3659(87)90034-4.
[70] S. Bochenek, F. Camerin, E. Zaccarelli, A. Maestro, M.M. Schmidt, W. Richtering, A. Scotti, In-situ study of the impact of temperature and architecture on the interfacial structure of microgels, Nat. Commun. 13 (2022) 3744, https://doi.org/10.1038/s41467-022-31209-3.
[71] S. Bazban-Shotorbani, E. Dashtimoghadam, A. Karkhaneh, M.M. Hasani-Sadrabadi, K.I. Jacob, Microfluidic directed synthesis of alginate nanogels with tunable pore size for efficient protein delivery, Langmuir 32 (2016) 4996–5003.
[72] G.M. Whitesides, The origins and the future of microfluidics, Nature 442 (2006) 368–373.
[73] M. Richter, O. Piwocka, M. Musielak, I. Piotrowski, W.M. Suchorska, T. Trzeciak, From donor to the lab: a fascinating journey of primary cell lines, Front. Cell Dev. Biol. 9 (2021) 711381.
[74] T. Lugo, S. Myers, T.A. Nguyen, Isolation and characterization of equine lymph node endothelial cells, Vet. Sci. 12 (2025), https://doi.org/10.3390/vetsci12090905.
[75] E. Cenni, G. Ciapetti, D. Granchi, C.R. Arciola, L. Savarino, S. Stea, L. Montanaro, A. Pizzoferrato, Established cell lines and primary cultures in testing medical devices in vitro, Toxicol. Vitro 13 (1999) 801–810, https://doi.org/10.1016/S0887-2333(99)00058-2.
[76] R.J. Geraghty, A. Capes-Davis, J.M. Davis, J. Downward, R.I. Freshney, I. Knezevic, R. Lovell-Badge, J.R.W. Masters, J. Meredith, G.N. Stacey, P. Thraves, M. Vias, Guidelines for the use of cell lines in biomedical research, Br. J. Cancer 111 (2014) 1021–1046, https://doi.org/10.1038/bjc.2014.166.
[77] N.N. Silveira, H.E. Andrada, J.M. Paulino, N.C. da S. Boaretto, E.F. Molina, R.A. dos Santos, Unveiling biocompatibility: comprehensive study on Epoxy–polyetheramine-based polymeric nanogels in CHO-K1 cell line, Future Pharmacol. 5 (2025), https://doi.org/10.3390/futurepharmacol5030054.
[78] B. Saqafi, F. Rahbarizadeh, Effect of PEI surface modification with PEG on cytotoxicity and transfection efficiency, Micro & Nano Lett. 13 (2018) 1090–1095, https://doi.org/10.1049/mnl.2017.0457.
[79] M. Tamura, S. Ichinohe, A. Tamura, Y. Ikeda, Y. Nagasaki, In vitro and in vivo characteristics of core–shell type nanogel particles: optimization of core cross-linking density and surface poly(ethylene glycol) density in PEGylated nanogels, Acta Biomater. 7 (2011) 3354–3361, https://doi.org/10.1016/j.actbio.2011.05.027.